REPUBLIC OF TÜRKİYE

ALTINBAŞ UNIVERSITY

Institute of Graduate Studies

Mechanical Engineering

INVESTIGATION OF GEOMETRICAL AND STRUCTURAL DESIGN ON THE EFFICIENCY IMPROVEMENT OF SOLAR AIR HEATER

Ebrahim Abdulrahman Taresh AL-SAMEAI

Master’s Thesis

Supervisor

Asst. Prof. Dr. Yaser ALAIWI

İstanbul, 2025

INVESTIGATION OF GEOMETRICAL AND STRUCTURAL DESIGN ON THE EFFICIENCY IMPROVEMENT OF SOLAR AIR HEATER

Ebrahim Abdulrahman Taresh AL-SAMEAI

Mechanical Engineering

Master's Thesis

ALTINBAŞ UNIVERSITY

2025

The thesis titled INVESTIGATION OF GEOMETRICAL AND STRUCTURAL DESIGN ON THE EFFICIENCY IMPROVEMENT OF SOLAR AIR HEATER prepared by EBRAHIM ABDULRAHMAN TARESH AL-SAMEAI and submitted on 16/06/2025 has been **accepted unanimously** for the degree of Master of Science in Mechanical Engineering

Asst. Prof. Dr. Yaser ALAIWI
Supervisor

Thesis Defence Committee Members:

Asst. Prof. Dr. Yaser ALAIWI	Department of Mechanical Engineering, Altınbaş University	_______________
Asst. Prof Dr. İbrahim KOÇ	Department of Mechanical Engineering, Altınbaş University	_______________
Asst. Prof Dr. Haydar İzzettin KEPEKÇI	Department of Mechanical Engineering, İstanbul Gelişim University	_______________

I hereby declare that this thesis meets all format and submission requirements for a Master's thesis.

I hereby declare that all information/data presented in this graduation project has been obtained in full accordance with academic rules and ethical conduct. I also declare all unoriginal materials and conclusions have been cited in the text and all references mentioned in the Reference List have been cited in the text, and vice versa as required by the abovementioned rules and conduct.

Ebrahim Abdulrahman Taresh AL-SAMEAI

Signature

DEDICATION

I would like to express my gratitude to Assistant Professor Dr. Yaser AlAIWI, Lecturer at ALTINBAŞ University, Department of Mechanical Engineering, who supervised my research and provided valuable assistance in the field of scientific research. I would like to thank Associate Professor Dr. Suleyman BAŞTURK, Head of the Department of Mechanical Engineering at ALTINBAŞ University, and the rest of the teaching staff for their contribution to the success of this scientific journey. I'd also like to thank all of my friends for their encouragement, advice, and knowledge.

ABSTRACT

INVESTIGATION OF GEOMETRICAL AND STRUCTURAL DESIGN ON THE EFFICIENCY IMPROVEMENT OF SOLAR AIR HEATER

AL-SAMEAI, Ebrahim Abdulrahman Taresh

M.Sc., Mechanical Engineering, ALTINBAŞ University,

Supervisor: Asst. Prof. Dr. Yaser ALAIWI

Date: 06 / 2025

Pages: 73

This study aims to enhance the thermo-hydraulic performance of solar air heaters (SAHs) by employing various broken V-shaped artificial roughness configurations on the absorber plate, with and without incorporating grooves of triangular, semi-circular, and trapezoidal cross-sections. A three-dimensional numerical analysis was conducted using ANSYS Fluent software to examine the fluid flow and the heat transfer characteristics within a solar air heater duct with an aspect ratio of 12 and a hydraulic diameter of 0.046 m, across Reynolds numbers ranging from $3*10^3$ to $15*10^3$. Geometrical parameters of roughness are set to the optimized and best performance of related experimental validated set of parameters.

The results indicate that there is significant increase of both heat transfer rates and friction losses of V-shaped ribs attributed to enhanced turbulence and vortex formation. Applying gaps in the V-ribs yield further enhancement in Nusselt numbers, accompanied by slight increase in friction factors. The maximum improvement in the Nusselt number reaches three times greater than that of a smooth duct, with an increase of THPP ranging from 2 to 2.15.

Furthermore, the addition of grooves to the broken V-ribs configurations increases both Nusselt numbers and friction factors. For the semi-circular grooves, which provide the most favourable results, the Nusselt number reaches up to 1.25 times that of the corresponding arrangement without grooves, with only a slight increase in friction factors. THPP of the combined V-rib and groove arrangements significantly exceed those of other configurations, with maximum values observed for V-ribs combined with semi-circular grooves, ranging from 6.3 to 2.4, depending on the Reynolds number.

Keywords: Artificial Roughness, Broken V-ribs, Grooves, Solar Air Heater (SAH), Performance Enhancement.

TABLE OF CONTENTS

Pages

ABSTRACT .... **vi**

LIST OF TABLES .... **x**

LIST OF FIGURES .... **xi**

ABBREVIATIONS .... **xiii**

LIST OF SYMBOLS .... **xiv**

1. INTRODUCTION **1**

1.1 RESEARCH BACKGROUND 1

1.2 RESEARCH PROBLEM 8

1.3 RESEARCH OBJECTIVE 9

1.4 THESIS STRUCTURE 9

2. LITERATURE REVIEW **11**

3. METHODOLOGY **25**

3.1 COMPUTATIONAL FLUID DYNAMICS 25

3.2 GOVERNING EQUATIONS 26

3.3 THPP ANALYSIS 28

3.4 CASE STUDY AND METHODOLOGY 29

3.4.1 Geometry and Computational Domain 30

3.4.2 Generation of Mesh 32

3.4.3 Boundary Conditions 33

3.4.4 Numerical Settings 35

3.4.5 Results Validation 35

4. RESULTS AND DISCUSSIONS **37**

4.1 BROKEN RIBS WITHOUT GROOVES 37

4.1.1 Heat Transfer Analysis 39

4.1.2 Friction Analysis 42
4.1.3 THPP 44
4.2 COMBINED BROKEN V-SHAPED RIBS AND GROOVES 45
4.2.1 Heat Transfer Analysis 46
4.2.2 Friction Analysis 49
4.2.3 THPP Analysıs 51
5. CONCLUSION AND FUTURE WORK 53
5.1 CONCLUSION 53
5.2 FUTURE WORK 55
REFERENCES 56

LIST OF TABLES

Pages

Table 3.1: Values of Duct, Roughness, and Flow Parameters 31

Table 3.2: Boundary Conditions Imposed on the Computational Domain 34

Table 4.1: Values of Duct and Roughness Parameters.. 39

LIST OF FIGURES

Pages

Figure 1.1: Global Horizontal 2

Figure 1.2: SAH Schematic Diagram 3

Figure 1.2: SAH Schematic Diagram 4

Figure 1.4. Schematic Representations of SAH: (a) Single-pass, (b) Double Pass Parallel Flow, (c) Double Pass Counter Flow, (d) Double Pass Recycle Flow 4

Figure 1.5: (a) Porous and (b) Non-porous Absorber Plate 5

Figure1.6: Effect of Roughness Elements on Flow Field 6

Figure 1.7: Catalogue of Artificial Roughness Geometry 7

Figure 3.1: The SAH Geometrical Model -the Computational Domain. 31

Figure 3.2: Grid Independence Test 32

Figure 3.3: Computational Domain’s Mesh 33

Figure 3.4: The Surface Names and Boundary Conditions 34

Figure 3.5: Nu Number Comparison with Reference Expermental Results 36

Figure 3.6: Friction Factor Comparison with Reference Experimental Results 36

Figure 4.1: The SAH Geometrical Model- 3D View 38

Figure 4.2: The SAH Geometrical Model - 2D View with Naming Key Duct and Roughness Parameter 38

Figure 4.3: Nu Number Change with Re Number for Broken V- shaped , Continuous V-shaped Ribbed Ducts, and Smooth Ducts. 40

Figure 4.4: Velocity Vector for a Continuous V-shaped Ribbed Duct at Re = 9000. 41

Figure 4.5: Velocity Vector for Broken V-shaped Ribbed Duct at Re= 9000 41

Figure 4.6: Friction Factor Variation with Re for Broken V-shaped, Continuous V-shaped Ribbed Ducts, and Smooth Ducts. 43

Figure 4.7: THPP Variation with the Re Number for Broken and Continuous V-shaped Ribbed Ducts 45

Figure 4.8: The SAH Geometrical Model - (rib-groove) Arrangment 46

Figure 4.9: Nu Variation with Re for Roughened Ducts with Various Arrangements: Broken V-Shaped ribs and Combined Broken V-shaped ribs and Grooves of Triangular, Circular and Trapezoidal Shapes 47

Figure 4.10:Temperature Contour for the case of Discrete V-ribs with Circular Groove at Re=3000 48

Figure 4.11: Velocity for the case of Discrete V-ribs with Circular Groove at Re=15,000 49

Figure 4.12: Friction Factor Variation with Re for Broken V-ribs without Grooves and for the Different Broken V-ribs- grooves Combinations. 50

Figure 4.13: THPP Change with Re Number for Broken V-ribs without Grooves and for the Different V-ribs- Grooves Combinations 51

ABBREVIATIONS

CFD	:	Fluid Dynamics
GHI	:	Global Horizontal Irradiation
Nu	:	Nusselt Number
PCM	:	Phase Change Material
Re	:	Reynold Number
SAH	:	Solar Air Heater
THPP	:	Thermal Hydraulic Performance Parameter

LIST OF SYMBOLS

D_{hi}	:	Hydraulic Diameter
μt	:	Turbulent Viscosity
K	:	Turbulent Kinetic Viscosity
h	:	Convective Heat Transfer Coefficient
e	:	Ribs Height
P	:	Roughness Pitch
σt	:	Turbulent Prandtl Number
Q_u	:	Rate of Useful Heat
T_w	:	Absorber Plate Temperature
T_b	:	Bulk fluid Temperature
e/D	:	Relative Roughness Height
P/e	:	Relative Roughness Pitch
G/e	:	Relative Gap Width
D_h	:	Hydraulic Diameter
α	:	Attack Angle
G_d/L_v	:	Relative Gap Distance
S'/S	:	Relative Staggered Rib Length
P'/p	:	Relative Staggered Pitch Position
d/w	:	Relative Gap Position

1. INTRODUCTION

1.1 RESEARCH BACKGROUND

In recent years, energy is regarded as a driver of progress and development, and energy consumption continues to increase due to the growth of human and economic activities. Coil, oil, gas, and other traditional energy sources are finite and gradually depleting; it is anticipated that they will not be sufficient enough to satisfy the world needs of energy for more than the next 70 years [1]. As a result of scarcity of traditional energy sources, fuel prices are likely to continue rising over the coming years, leading to even higher costs in the long term. Furthermore, the environmental concerns arising from the harmful emissions of fossil fuels are equally important alongside the concern of rising energy costs. The increasing pollution levels and their serious impact on human health, make it necessary to find a solution, which requires long-term sustainable approaches. Renewable energy projects have received increasing global attention due to their economic and environmental advantages. They are capable of meeting future electricity demands with less reliance on fossil fuels, reduce harmful gas emissions, and help address climate change. Solar energy is certainly the most abundant renewable energy source, as it is the origin of many of them, such as wind and tidal energy, which are caused by temperatures variations in different regions of the earth [2]. Over the years, solar energy has found applications in various areas, including drying processes, heating, cooling, and ventilating buildings, desalinating water for drinking, producing hot air and water for different purposes, generating electricity, and many others. The most well-known energy source for the future is solar energy, due to its remarkable characteristics. It is sustainable, free from air pollution, cost-effective, and an abundant source of energy [2],[3]. By the year 2025, it is predicted that solar energy will account for approximately 60% of world's energy demand, resulting in a 75% reduction in carbon releases compared to levels records in 1985 [4].

A huge amount of free sunlight reaches the earth every day, with the potential to produce an estimated 105 TW of energy, which far exceeds future global energy needs. The amount of sunlight received varies significantly based on geographical coordinates and weather conditions [5]. Yemen is situated in the southwestern corner of the Arabian Peninsula, within the earth solar belt, and hence has one of the highest solar radiation rates in the world. The daily solar radiation rate varies from 5.4 to 7.0 kWh/m^2/day, with daily sunshine hours ranging from 7.3 to 9.1 hours [6]. Figure 1.1 illustrates the solar radiation intensity across different cities in Yemen. It is evident that the country has a promising future for solar energy investment, and increased research and development activities should be dedicated to this area.

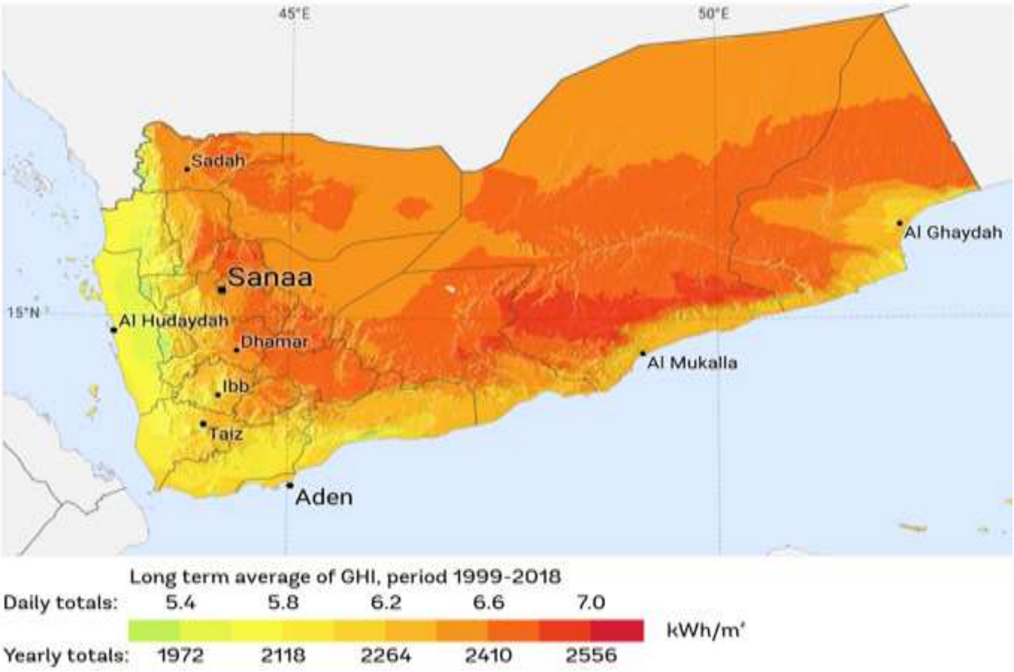

Figure 1.1: Global Horizontal Irradiation (GHI) in Yemen by Solar GIS Map [7]**.**

Converting solar energy into thermal energy is the simplest and most effective way to do . In essence, SAH is a heat exchanger that converts incoming solar radiation into heat that the working fluid (air) can carry. There are several uses for the hot air that is generated. like drying of foods, heating spaces, desalination, and ventilation and air conditioning [8],[9].There are many shapes and constructions available for SAH, but they all share two main characteristics: an absorbing plate and a working fluid. Figure 1.2 demonstrates a conventional SAH consisting of an insulated air duct, a glass cover, and an absorber plate. The absorber plate is built of a material has high thermal conductivity commonly from aluminum, copper, or steel. The cover is constructed from glass or other transparent material with high transmissivity and low absorptivity, allowing incident solar radiation to penetrate and reach the absorber plate. Heat is transferred from the absorber plate to the air flowing through the collector primarily by convection. The hot air duct is insulated to reduce the heat losses to the surroundings [10], [11].

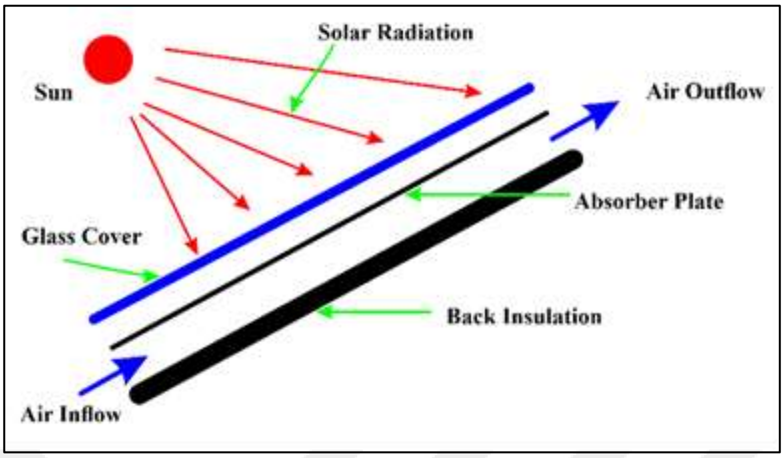

Figure 1.2: SAH Schematic Diagram [11].

SAH can be categorized into various types based on the absorber plate design, the number of collectors passes, the number of glazing used and the flow type, as illustrated in figure 1.3. Depending on the number of passes, SAH can primarily be categorized by flow path to single and double-path category. While there is one flow channel in a single pass SAH, the flow is passing in both ways of the heater plate in double pass SAH. Double-pass SAH is further classified into parallel flow, a counter flow (or crossflow), and a recycle flow, according to the directions of the airflow. In parallel flow SAH, the two air streams move in the same direction, while in counter flow SAH, the air flows in opposite directions. The recycle flow SAH principle is similar to that of the counter flow SAH, but it involves mixing a portion of the produced hot air that leaves with the incoming air, enhancing convective heat transfer [12],[13].Figure 1.4 illustrates schematic representations of the single-pass and the different designs of the double-pass SAH. It is common to utilize multiple glass covers, particularly in circumstances of high ambient temperatures and high wind speeds, to lower heat losses from the collector and consequently improve overall efficiency [14],[15].Finally, SAH can also be classified based on the type of absorber plate into non-porous and porous categories. Air flows through the plate in the porous type, whereas the air doesn't flow through the absorber plate in the non-porous type [16].Figure 1.5 illustrates the porous and non-pours SAH.

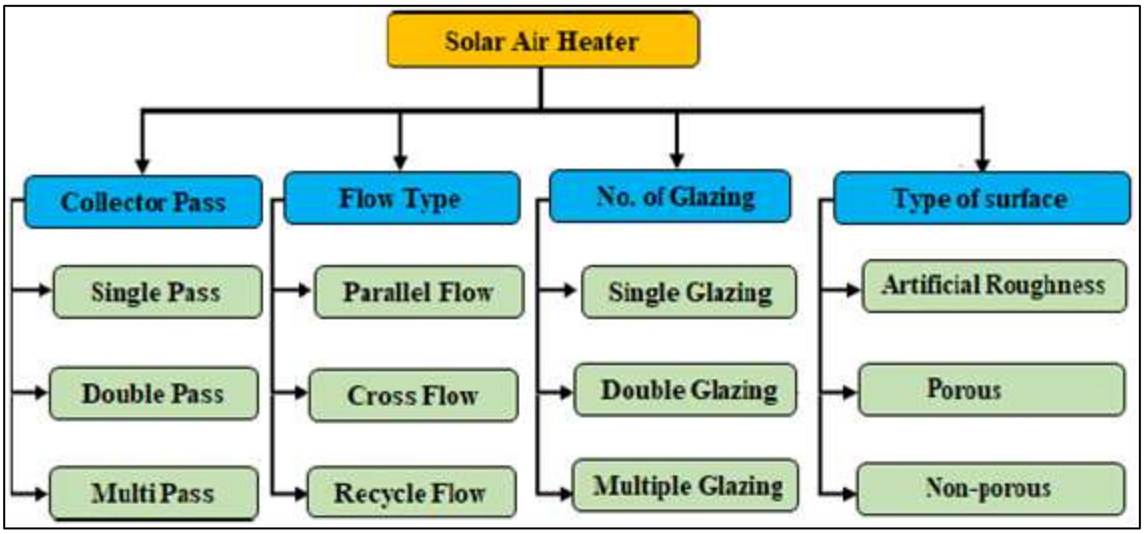

Figure 1.3: Solar Air Heaters' Classifications [12].

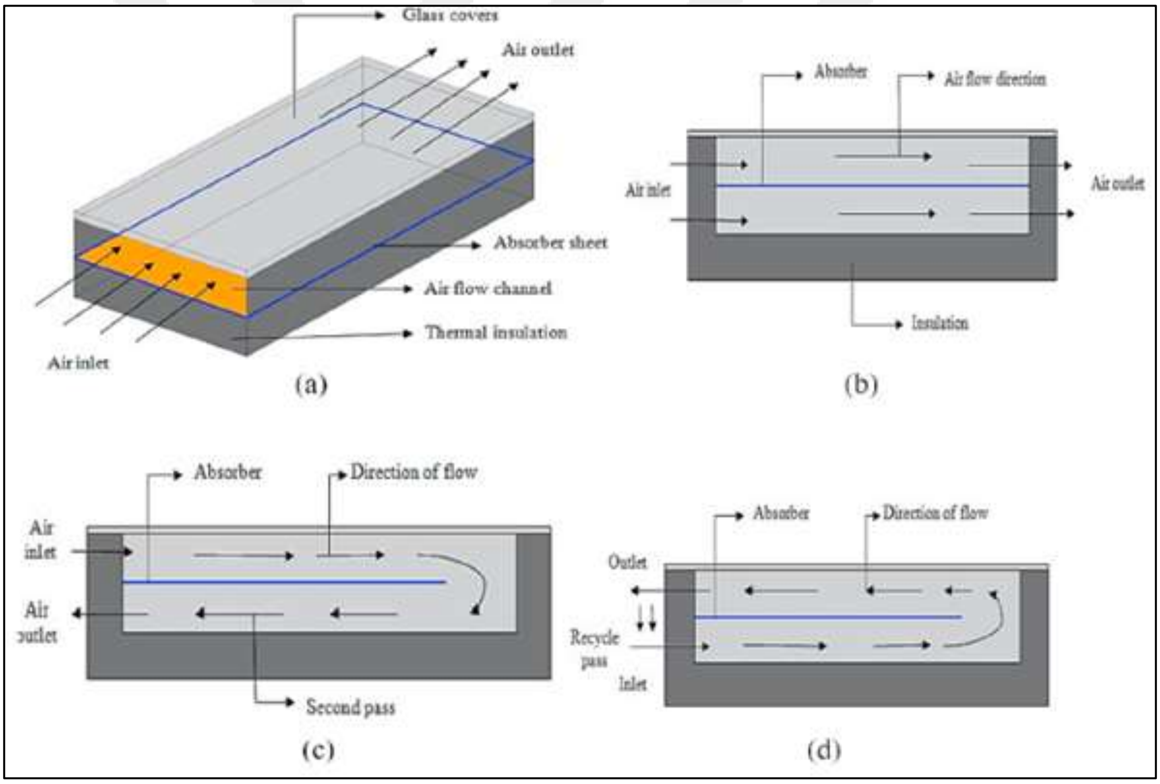

Figure 1.4 : Schematic Representations of SAH: (a) Single-pass, (b) Double Pass Parallel Flow, (c) Double Pass Counter Flow, (d) Double Pass Recycle Flow [13].

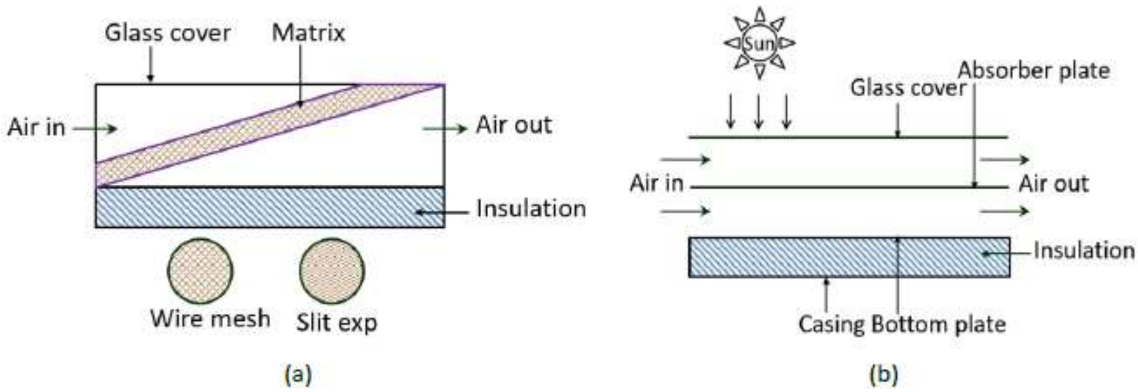

Figure 1.5: (a) Porous and (b) Non-Porous Absorber Plate [17].

The SAH has various advantages, including a simple design, low operating costs (beyond the initial capital investment), minimal maintenance requirements, and no concerns about leakage or corrosion compared to liquid collectors. However, SAHs are limited by their relatively low thermal performance[18].Several factors contribute to this significant drawback, including:

a. Poor thermal properties of air.

b. Restricted surface area of the absorber.

c. Minimal convective h between the air and the absorber plate.

d. Brief residence time of airflow within the collector.

e. Heat losses due to radiation.

f. Properties of the layer that in contact with heater plate.

Consequently, numerous theoretical and experimental studies have been conducted to address these challenges and improve the thermal performance of SAHs. Both active and passive ways were utilized for this target. Some effective engineering solutions include:

a. Developing innovative designs by roughening the surface, often through the incorporating artificial regular geometric roughness elements.

b. Applying selective coatings to the surface to reduce radiation losses.

c. Enhancing the thermal properties of the heat carrier fluid (the air) by introducing nanoparticles.

d. Applying PCM in order to store thermal energy.

The current study aims to improve heat transfer from the surface by using passive techniques that typically involve surface modification, like adding fins and/or ribs in various configurations. These modifications can enhance the overall efficiency of SAH by improving the THPP. Introducing artificial roughness elements to the absorber's surface induces turbulence in the flow adjacent to this surface. This considerably aids in breaking the thin laminar sublayer adjacent to the heat transferring surface, hence improving h. [19].Figure 1.6 illustrates that the air flow behavior is affected by of the roughness elements, The separation and reattachment of the boundary layer between adjacent elements significantly enhance surface heat transferring rates. The figure indicates that the characteristics of the roughness elements, including pitch distance and height, play a critical role in shaping the flow field within the viscous sublayer [20]. It is essential to note that introducing artificial roughness elements may result in increased pressure drops across the collector, which could negatively impact the energy needed to sustain the same airflow rate. Consequently, any improvements in thermal performance achieved through roughness techniques must be carefully balanced against potential pressure losses in these scenarios [21].

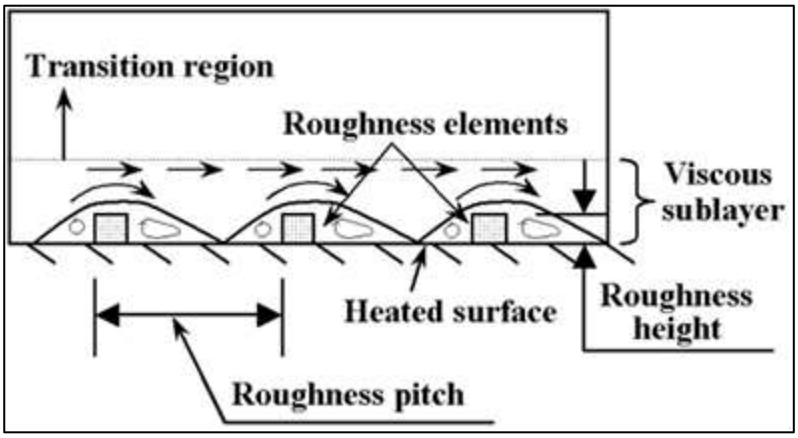

Figure1.6: Effect of Roughness Elements on Flow Field [20].

Several types of surface roughness geometries, with different shapes, arrangements, and orientations, were employed to improve heat transfer rates from the absorber surface.

Furthermore, the primary geometric parameters of the roughness, such as the pitch-to-height ratio and the height-to-hydraulic diameter ratio, have been optimized to ensure that the enhancement in heat transfer does not lead to a significant increase in pressure drop across the collector [22]–[24].Figure 1.7 illustrates the basic geometry of various types of roughness elements, variations in their parameters, and possible elements shapes.

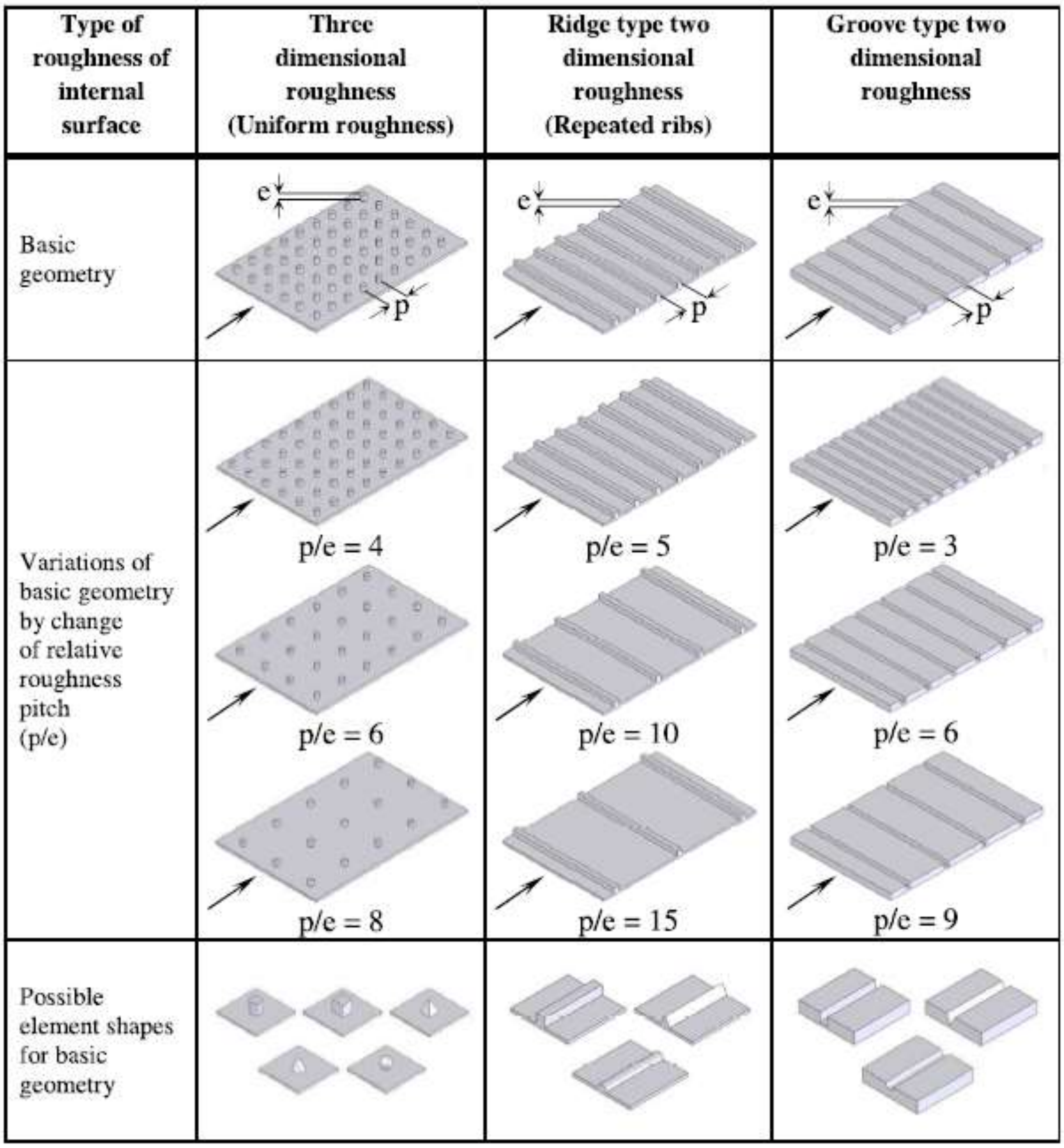

Figure 1.7: Catalogue of Artificial Roughness Geometry [25].

Nevertheless, enhancing the thermal performance of SAHs remains an area of active research. Further improvement can be achieved by exploring the various roughness geometry designs available in the literature and suggesting an optimal configuration with the best specifications. Computational Fluid Dynamics (CFD) provides a powerful tool for analysing the detailed flow dynamics and heat transfer behaviours in different complex geometries, particularly with the ongoing advancements in computational resources.

1.2 RESEARCH PROBLEM

Yemen experiences a severe energy crisis due to its limited fossil fuel reserves, and a complex political situation, which has devastating consequences for economic and people life. To overcome this challenge, a transition to renewable energy sources is crucial. Yemen geographical location offers an exceptional solar potential, with an estimated capacity of 400 GW, significantly exceeding its current energy needs. Although the country solar energy sector is still in its early stages, its ambitious plans are inspiring, despite the challenges it faces [26].

SAH is a basic device made to capture solar energy by collecting solar radiation and transforming it into thermal energy to be carried by the flowing air. However, SAHs suffer from low thermal performance because of the minimal thermal properties of the air, the low convective h between the flowing air and absorbing plate, and the thermal resistance resulting from the thin laminar sublayer in contact with the heater plate. Due to their wide range of remarkable applications, great efforts have been made from both researchers and industrial activities to improve the thermal efficiency of SAHs. Different approaches have been employed, including design modifications, the use of nanofluids, and the implementation of PCM for energy storage. A detailed review of the relevant studies focusing on the first approach, which is followed in this study, will be provided in Chapter Two. All investigations have confirmed that introducing the geometries of artificial roughness can considerably enhance the thermal efficiency of conventional SAHs. Although many roughness shapes with different parameters have been examined, every design presented had its limitations. Thus, the matter remains an active field of research, and there is always work to be done for further improvement. This study approaching further enhancement of the thermal performance of a SAH featuring V-shaped roughness geometry. While the effects of geometric parameters and operating conditions have been extensively investigated in previous researches, this study primarily focuses on modifying the roughness geometry. Specifically, grooves of different shapes are introduced in an attempt to achieve optimal heat transfer rates. Additionally, the impact on pressure drops across the collector, and consequently, on the consumed power, is also included in this investigation.

1.3 RESEARCH OBJECTIVE

This research includes a numerical investigation utilizing ANSYS Fluent software with the main goal of improving the THPP of the SAH by modifying the V-shaped geometry of the heater plate's artificial roughness. Friction factors and Nu numbers results are obtained and analyzed for various flow conditions for determining the most efficient design. The specific targets of this study can be concise as follows:

a. To inspect the existing V-shaped roughness designs in SAHs and identify areas for potential thermal performance improvement.

b. To assess the result of modifying the roughness geometric arrangement on the heat transmission and flow characteristics and identify the optimal configuration.

c. To calculate how operating parameters like Reynolds and flow rate affect heat transmission, pressure drop, air exit temperature, and collector efficiency.

1.4 THESIS STRUCTURE

In Chapter 1, a general background is provided, including an introduction to solar air heaters, their classifications, and the factors influencing their thermal performance. The study's problem statement and research goals are also presented in this chapter.

In Chapter 2, a thorough literature review is provided, focusing on previous studies that used artificial roughness geometries to improve heat transfer in SAH. Various roughness designs are analysed to understand the previous contributions toward improving the thermal performance of SAHs. The chapter concludes by summarizing the main findings from the literature review and identifying areas for improvement in the current study.

In Chapter 3, the methodology of the research is outlined, including the governing equations and turbulence models, numerical procedures, and validation against a reference experiment study. The chapter describes geometry build-up, meshing, boundary conditions definition, and numerical settings.

In Chapter 4, the detailed simulation results are presented, analysed and discussed. The effect of V-shaped roughness geometry parameters on the thermal performance of the SAH is explored. The heat transfer coefficient, pressure drop and exit temperature variations are examined and discussed. Additionally, the SAH performance is calculated, and the optimal arrangement is identified.

In Chapter 5, the main conclusions will be drawn based on the research findings, and recommendations for the future research will be provided.

2. LITERATURE REVIEW

Solar air heaters have recently gained significant popularity due to their practicality and wide range of applications. A major challenge associated with traditional smooth SAHs is their inefficient performance, primarily attributed to the existence of a viscos sublayer close to the heater plate. Enhancing the performance of SAHs by disturbing this sublayer has been a goal of extensive recent research. Researchers have investigated various factors that affect SAH efficiency in order to optimize its performance. These factors have included not only modifying to the shape and configuration of the absorber plate but also controlling the operating conditions, flow patterns, and design parameters. Since this study aims to enhance SAH thermal performance by modifying the absorber plate with V-shaped roughness elements, this chapter focuses on recent literature concerning surface shape modification, particularly those employing V-shaped roughness designs. The chapter also includes a brief discussion of other roughness geometries to better identify the research problem. The review covers both experimental and numerical investigations, aiming to deepen a thorough comprehension of heat transmission and flow dynamics in SAHs.

Traverse ribs are among the simplest roughness elements utilized to improve turbulence over the absorber plate, therefore enhancing rates of transferred heat. One of the early investigations in this area was conducted in [27],which examined the impact of applying small diameter wire geometries on thermal performance of SAH. The results revealed that introducing such roughness elements could enhance the Nu number up to 2.38 times in comparison to that of a smooth SAH. However, this improvement in heat transfer was associated with a notable rise in the friction coefficient, which reached a factor of 4.25. Furthermore, the results showed a considerable impact of roughness parameters, such as p/e and e/D on both friction factor and heat transfer. Authors employed similar experiment instrumentation to investigate the combined effect of p/e, e/D, and Re number THPP of SAHs in [28]. The results revealed that optimal THPP of 71% can be obtained at a roughness Reynolds number, defined as, $e^{+} = e/D\sqrt{f_r/2}\,Re$, with a corresponding value of 24.

A SAH with 90^{o} broken transverse ribs absorber plate was utilized by researchers to enhance heat transfer rates[29]. It was noticed that the maximum improvement in convective h was close to 1.4 times that of the smooth SAH, reached at a pitch = 20 mm. In other studies, experimental and numerical study was also carried out to test the impact of using multiple broken traverse ribs on the THPP of a SAH. The roughness elements arrangement used in their investigation, with roughness parameters of e/D = 0.043 and P/e = 10 was employed [30]. The findings revealed that the maximum heat transfer improvement reached more than 300% that of a smooth duct, achieving a maximum thermal efficiency of 72.25% in comparison to 44.26% for traditional SAH. The optimal THPP for the proposed ribbed arrangement was found to be 2.10.

According to a study, experimental work was applied to test the flow characteristics and heat transmission in a SAH with an absorbing plate incorporated with roughness ribs arranged with inclined patterns. The results showed that inclined ribs delivered better THPP compared to traverse ribs. The optimal THPP was found at $\alpha = 60^o$, a e/D of 0.033, and a corresponding Re number of $14*10^3$ [31]. It's also tested the effect of inclined parallel ribs on flow behaviour and heat transmission, applying these ribs to one wall during some experiments and to both opposite walls of the duct during others [32]. The roughness pitch varied between 6.66 and 20, while maintaining other roughness parameters fixed at $\alpha = 45^o$ and e/D $9*10^{-2}$ Results revealed that the optimal heat transfer took place with a p/e between 6.66 and 10 for both sides ribbed duct and at 13.33 relative roughness pitch of single ribbed wall duct. The Nusselt number peaked at 2.25 and 2.55 times more than that of smooth wall for one ribbed wall and two ribbed walls respectively. However, there was significant increase in friction factor along with heat transfer enhancement ranged between 4.3 and 14.3 for the one-sided and two-sided ribbed walls, respectively [32] .

An investigation was carried out for the usage of significant repeated inclined squared ribs with a gap as artificial roughness to improve heat transmission and friction coefficient in SAHs [33]. Results indicated that the presence of the gap caused an increase in Nu number and friction coefficient magnitudes. The maximum values reached were 2.59 and 2.87 times greater than those belong to the smooth duct for the Nusselt number and friction factor, respectively, resulting in a THPP of 1.82. These maximum values were observed for gap specifications of d/W = 0.25 and g/e = 1. Furthermore, comparing these results with the continuous rib case revealed that Nusselt number and friction factor remarkably increased for G/e < 1 [33].

Other researchers also employed a 60º inclined discrete rib arrangement on the absorber plate's bottom side to improve heat transferring in a SAH to examine its impact on friction losses and heat transmission. absorber plate roughened with the targeted arrangement indicated enhancement of Nu number by 257% compared to the smooth plate, but this improvement was parallelly associated with a friction factor increasing by less than 4 times [34]. The friction coefficient and Nu number were found to be functions of the rib and gap parameters, with maximum values achieved at P/e= 12 and e/D = $4.98*10^{-2}$. Furthermore, other researchers introduced staggered ribs before the gaps in their experiments, the results revealed that the staggered elements increased turbulence intensity compared to similar roughness arrangements without staggered elements, resulting in enhanced heat transfer rates. The Nusselt number reached maximum values of 3.29 times compared to the smooth plate. At these optimal roughness parameters, the THPP achieved its maximum value of about 2 [35].

V-shaped roughness can be considered as a result of two inclined rib roughness combined together. When inclined ribs are present, the resulting vortices move in a spanwise direction and cover a long distance towards the trailing edge. In contrast, with V-shaped roughness, the vortices take a shorter path toward the center of the plate. This characteristic might further enhance heat transfer rates by maintaining high temperature gradients and by creating additional turbulence through improved vortex mixing. Extensive investigations have explored various V-shaped roughness arrangements to determine the effects of their shapes and parameters on the THPP of SAH. The most significant experimental and numerical studies conducted in this area are presented in this section.

Extensive experiments were done to see how rib angle and orientation affected heat transmission and pressure drop in a square channel with two roughened walls on opposite sides, across a wide range of Reynolds numbers. The experiments utilized various rib configurations, including V-shaped ribs at angles of 45°, 60°, 90°, 120°, and 135°. The findings indicated that the V-shaped arrangements, especially the 45° and 60° ones, improved thermal performance and heat transfer the most compared to the other configurations that were looked at. THPP of these arrangements reached a value of 1.4, and the heat transfer enhancement exceeded that of the full rib case (90° ribs) by up to 79% [36],[37].

In a different study, scientists used an experiment to look at how heat moves and how much friction is lost in a SAH that has V-shaped ribs on bottom of heater plate. The research aimed to assess the effect of Reynolds numbers varying from $2.5*10^2$ to $18*10^3$, e/D from 0.02 to 0.034, on SAH performance while P/e kept at 10. Results revealed that both Nu number and friction coefficient augmented significantly by increasing Reynolds number, with a more remarkable increase in the friction factor. Max. Enhancement in Nu number and friction coefficient reached more than two times and about 3 times, in order, compared to those in a smooth duct. We observed these values at the highest tested Reynolds number, α =60°. However, the performance declined when the angle of attack was > 60°. On the other hand, comparing these findings to those of inclined rib roughness, it was noted that Nusselt number improvement was less, at 1.14, Nevertheless, it continued to emphasize the benefits of the V-shaped roughness features in comparable operating circumstances. [38].

Various kinds of artificial roughness geometries were utilized in an experiment to see how they could help heat transfer in SAH. These included traversing and inclined repeated ribs, as well as V-up \ down continuous and detached ribs. The parameters of these roughness geometries include a P/e =10, e/d varying from $4.67*10^{-2}$ to $5*10^{-2}$, and α = 60 degrees for the inclined ribs and V-pattern arrangements. All the examined arrangements significantly enhanced heat transfer, according to results, V-down discrete ribs arrangement showed the biggest improvement. The maximum increase in Stanton numbers reached as high as 142% compared to a smooth plate. Furthermore, the discrete V-shaped configurations exhibited minimum friction loss compared to other continuous ribbed arrangements, due to changes in flow behaviour [39].

Similarly In the same way, Convective h and friction factor have been looked at when different types of V-ribs were put on the bottom of the SAH absorbing plate. For the research, many tests were done with different roughness parameters, such as P/e = 6–12 with Reynolds numbers varying from $2*10^3$ to $20*10^3$. Findings showed that the absorber plate roughened with multiple V-ribs enhanced the Nusselt number 6 times more than a smooth duct. However, the friction factor could also reach up to five times that of a smooth duct. The optimal THPP was observed for the roughness parameter P/e = 8 and conversely, the friction factor was observed to increase monotonically with W/w and e/D, while reaching a maximum value at $\alpha = 60°$ and P/e = 8. The friction factor kept going up when the relative roughness width (W/w) went up. This was because flow separation created vortices [40].

It was also tested in another study to see how heat moves and how much friction there is in a SAH duct with a 12:1 aspect ratio and a roughened absorber plate with separate V-down ribs, Reynolds numbers varied from $3*10^3$ and $15*10^3$. The study examined variations in d/w, g/e, α, e/d and p/e. it was discovered that the discrete V-down ribs improved heat transfer more than a continuous V-down ribs arrangement with the same specifications. The presence of a gap raised the flow velocity, hence Nusselt number improved downstream of the gap. It was seen that the Nusselt number got better by about 3 times more than smooth duct when P/e = 8. Heat transfer rates were noted to decrease on both sides of these optimal roughness parameter values. It was observed that introducing the roughness caused an increments in friction factor values, reaching up to more than 300% compared to a smooth duct [41]–[43].

Another study looked at how making absorber plates roughened with staggered and broken V-shaped ribs improved friction loss and heat transmission rates in SAH. The tests were done with Reynolds numbers from $3*10^3$ to $17*10^3$, while (p'/p) varied from 0.2 to 0.8 and the (s'/s) ranged from 0.2 to 0.8. What the findings showed was that the studied roughness geometry works better than the continuous V-shaped ribs and the discrete configuration without staggered ribs. We attributed this to the enhanced turbulence the staggered ribs caused. A maximum increase in Stanton number of 3.12 was observed when comparing it to that of a smooth duct, at roughness parameters s'/s = 0.6 and p'/p = 0.6 [44].

Authors presented experimental results on friction coefficient and Nu numbers in a SAH with an absorber plate incorporating multi-V-shaped, gapped ribs roughened plate, test carried on a Reynolds number varying from $2*10^3$ to $2*10^4$. A roughened wall used in the experiments, while considering the key roughness parameters' effects on the SAH thermal performance. The parameters examined included P/e from 6 to 12, W/w from 1 to 10, g/e from 0.5 to 1.5, G_d/L_v from 0.24 to 0.80, and α from 30^o to $75°$.The research demonstrated that the artificial roughness significantly magnified both the Nu number and the friction coefficient to be maximum at about six times, more than those found in a smooth duct. These optimal performance values were achieved with the following roughness parameters: $\alpha = 60^o$, e/D = 0.043, W/w = 6 and g/e = 1.0 [45].

A V-shaped, symmetrically gapped roughened plate was used on SAH for heat transfer improvement. The experiments have been conducted at Re\numbers varying from 4000 to $18*10^3$, with roughness parameters related to a varied g/e from 1 to 5, number of gaps (Ng) from 1 to 5, e/d= 0.043 and α from 30^o to 75^o. Results revealed that the Nu number increased approximately 3.6 times due to the roughness geometry compared to smooth duct, however, friction coefficient also increased by a similar magnitude. The optimal results were obtained for the geometrical specification of $\alpha = 60^o$ [46].

Experimental research was conducted on heat transmission improvement in a SAH duct with a 12:1 aspect ratio, using discrete V-down, and staggered artificial roughness ribs. The roughness parameters were as follows: P/e ranging from 4 to 14, and α from 40° to 80°, while p/P, w/e and g/e were held constant at 0.65, 1, and 4.5, respectively. The experiments have been done for Re numbers varying from $4*10^3$ to $12*10^3$. The results indicated both Nu number and friction coefficient values significantly increased compared to smooth plate values, attributed to turbulence, flow acceleration, secondary flow, and the phenomena of detachment and reattachment of flow resulted from the roughness [47]. Maximum Nu number was observed to reach its highest values for e/D of 0.044, while maximum friction coefficient value was noted for e/D of 0.057. The study revealed that, in contrast to previous research, increasing the e/D > 0.044 caused a decrease in Nusselt number, while the friction coefficient kept increasing with higher e/D values. Maximum improvement in Nu number was 3.34 times that of a smooth plate, and THPP reached a value of 2.45.

A three-dimensional numerical study was done to examine flow measurements and heat transmission in a SAH with multi-V-shaped ribs on its absorbing plate, using ANSYS Fluent 14.0 software with the RNG k-ε turbulence model. In a SAH duct used in the simulation, where the impact of the roughness parameters on heat and flow fields was considered. The e/D was varied from 0.03 to 0.11, W/w from 3 to 10, P/e from 3 to 20, for Reynolds number values ranging from $8*10^3$ to $20*10^3$[48]. The numerical simulation demonstrates the presence of streamwise helical vortex flows generated by the multi-V-shaped roughness elements, which enhance flow mixing near the absorber plate, along with a secondary vortex structure observed in the region between ribs. The increased mixing of fluid significantly contributed to the rise in both Nu number and friction coefficient compared to the corresponding values in a smooth duct, resulting in a maximum THPP of 1.93 occurred at Re =8000, e/D =0.03, and α = 45° [48].

In a subsequent study, a similar working section and ribs arrangement were used, focusing on determining the optimal number of, and the effect of roughness geometrical parameters on fluid dynamics and rates of heat transferred. The conclusion confirmed that the multiple V-shaped ribs arrangement has a significant positive effect in improving heat transmission, due to increased fluid mixing adjacent to the absorber plate. A THPP found to be maximum at a factor of 2.35 for the optimal selection of the span wise rib number, which varied with the different rib parameters. It was reported that increasing α , p/e and H , resulted in a decrement in the optimal number of spanwise ribs, while e/d had a limited effect, especially at higher values [48].

Similarly, a numerical study on heat transmission and flow structure in a SAH featuring various V-pattern rib shapes was presented, with Reynolds numbers varying from 4000 to $24*10^3$ ribbed geometries included in the simulation, using parameters of P/e =10 and e/D =0.040. Ansys Fluent software using RNG k-ε for modelling turbulence to resolve the governing equations. The results highlighted that all examined V-pattern ribs shapes significantly improved thermal performance compared to a smooth plate, with the greatest enhancement obtained for the multi-V-pattern, staggered ribs with grooves roughness shapes. The THPP reached 3.67 within the range of investigated parameters [49],[50].

In the same way, researchers worked on numerical simulation on flow dynamics and heat transmission in a SAH with an inline and staggered multiple V-shape roughened duct incorporating different design parameters. These parameters have been used and compared in the numerical investigation. The key flow and rib parameters were e/D_h = 0.043, p/e = 10, and Re = 10000.The staggered arrangement resulted in a better heat transfer improvements and overall THPP compared to the inline arrangement. The maximum Nusselt number and THPP factor in the staggered arrangement were greater than the corresponding values in the inline arrangement, by 26% and 18%, respectively. The gap flow in the staggered arrangement induced two opposing effects on heat transfer, therefore, optimizing the stagger distance was crucial for the heat transfer enhancement [51].

A comprehensive numerical and experimental analysis to improve flow measurements and heat transmission in a SAH, employing discrete V-shaped, staggered on the heater plate. About the roughness arrangement used in the investigations, the roughness geometrical parameters were as follows: P/e = 6 -14, e/D_h = 0.043. The flow conditions corresponded to Reynolds' numbers varying from $4*10^3$ to $14.5*10^3$. The results exhibited that the installed roughness resulted in a significant improvement in heat transmission rates and the THPP. Nu number and THPP enhancement reached 2.2 and 3.4 times more than smooth plate, orderly. Furthermore, the authors reported that the THPP obtained in their study was higher than that of all existing corresponding roughness arrangements. Maximum THPP of 1.59 was gained with a corresponding P/e = 10, and a Reynolds number slightly above 12000 [52],[53].

An examination of flow measurements and transferred heat in a double-pass SAH with detached multi-V-shaped, staggered rib arrangement on both surfaces of the heater plate, was conducted. Experiments have been conducted with varied Re number between 2000 and 20,000, while investigation covered the following roughness parameters: W/w from 5 to 8, r/e from 1 to 4, p'/p 0.2 - 0.8. Results showed a significant improve in Nu number accompanied with a considerable increment in friction coefficient values due roughness existence. Friction coefficient and Nu number reached maximum values at 3.13 and 4.52 times compared to those of smoot plate, respectively. Max. improvement was achieved at r/e = 3.5 [54].

An experiment was conducted to see whether a symmetrically gapped V-rib might enhance the transferred heat rates in SAH. The experiments have been conducted with a varied Reynolds numbers between 3000 and 14,000. The proposed roughness geometry featured a relative pitch varying from 10 to 16, with fixing the other parameters at r/e = 4 and p/e = 0.65. The results indicated that introducing the symmetrically gapped, staggered V-ribs provided further increase in both Nusselt number and friction factor. Specifically, friction factor and Nusselt number and for the V-rib with symmetrically gapped unstaggered ribs were determined to be 3 times and 2 times more than those for a smooth duct, respectively.

With the addition of the staggered ribs, these values increased to 3.13 and 2.3, respectively. Furthermore, the value of THPP also increased from 1.41 for the symmetrically gapped, unstaggered V-ribs to 1.57 for the symmetrically gapped, staggered V-rib geometry. The optimal heat transfer rates and THPP values were matching a p/e of 12 [55].

In an investigation of the effects of incorporating a pattern of symmetrical gaps and staggered element geometry into the V-rib and its impact on THPP of a SAH. They employed a suggested roughness configuration in their experiments. They preserved the identical α, S/e and g/e, as in the previous study [55], [56].

Additional roughness parameters included P/e = 10, (Ng) number of main gaps equal to 4, P'/P =0.4, and d/w of the additional gap varying from 0.25 to 0.85. The studied Re number was ranged from $4*10^3$ to $15*10^3$. Results showed that the proposed arrangement provided improved THPP compared to the previous configuration. Maximum resulted Nusselt number was determined to be increased to 2.51 times more than the smooth plate, while maximum resulted friction coefficient value was found to be reduced to 2.7 times more than smooth plate. Consequently, the THPP increased to 1.82, compared to a value of 1.57 for the corresponding V-geometry arrangement without the additional gaps pattern. The optimum findings were observed at roughness parameter d/w = 0.65 [56].

The comparison of thermal performance of arc-shaped, gapped ribs with V-shaped, gapped ribs having the same parameters and operated in the same way, both of which were used to add repeated roughness to a SAH. A study examined the roughness of the ribs. Ansys software conducted the numerical investigation for Reynolds numbers varying from $3*10^3$ to$15*10^3$. The research also included an experimental validation study. The roughness parameters such as p/P, e/D_h , α were fixed at 0.65, 0.04, 60°, respectively. Results showed that the V-shaped rib roughness outperformed its peers of arc- shaped roughness significantly in terms of thermal performance. The V-shaped ribs Nu number improve was stated to be 4.05 for and 2.4 for the arc-shaped ribs, whereas the friction factor showed not much different values due to the roughness was quite similar for both rib types. The V-shaped ribs' THPP value was 2.21 and 1.5 for the arc-shaped ribs, further demonstrating the superior performance of the V-shaped design [57].

In another experimental study, the fluid flow dynamics and heat transmission of SAH were improved by incorporating interlocking twisted V-shaped ribs on absorber plate featuring test roughness .The experiments have been conducted for air massflow rates related Reynolds numbers ranging from $3*10^3$ to $21*10^3$, utilizing the following roughness parameters: S/e = 6.15–10.26, and P/e = 7–11. the considered roughness arrngement, along with the definitions of its parameters. The results demonstrated that the staggered, twisted V-shaped ribs significantly improved the heat transmission rate while only causing a minimal raise in pressure drop. Specifically, Nu number was noted to be raised by 3.43 times more than smooth plate, meantime friction factor rose by only 2.57 times in comparison to smooth duct. Best THPP was reported to be with the roughness parameter set at P/e = 9[57], [58].

A comprehensive numerical study to test the effect of a novel V-shaped roughness of a SAH's absorbing plate on heat transmission and dynamics of fluid flow was performed. Three-dimensional numerical simulation utilizing Ansys Workbench software using RNG k-ε turbulence model was used for Re varying between $4*10^3$ to $14*10^3$. The roughness geometry included a p/e ranged from 6 to 14 to evaluate the results of rib spacing on SAH efficiency. The results determined that Nusselt number significantly raised with increasing p/e until it reached a value of 10, after which it began to decrease. maximum Nusselt number enhancement, reached up to 76.2%, was observed at a Reynolds number of $12*10^3$[59].

Recently, Authors utilized a SAH featuring a V-shaped pattern, arranged with fins interrupted straightly and tested the impact of the SAH tilt angle on thermal performance. Four different tilt angles were examined: 0^o (horizontal position), 10^o, 20^o, and 30^o. The results indicated that the optimal tilt angle was 20^o, which resulted in the highest hot air exit temperature and energy efficiency compared to the other tilt angles tested. The hot air exit temperature increased by up to 15.7 % and energy efficiency enhanced by up to 38.2 % compared to the horizontal position [60].

A numerical simulation of a return air SAH containing V-type baffles to estimate its thermal performance under different artificial roughness parameters was conducted. The SAH and the V-type baffles utilized in the study. It was observed that both sides baffled absorber plate exhibited better efficiency compared to configurations where the baffle was placed above or below the plate. Furthermore, Thermal performance of the best-designed finned SAH increased by 33.7% compared to a similar design without baffles, and by 59.53% compared to an ordinary SAH of single flow without baffles [61].

Various types of artificial roughness were tested by researchers, including traverse, inclined, and V-shaped ribs, to improve flow characteristics and heat transmission in SAHs. For example, many researchers have been investigating arc ribs following the study of V-shaped ribs, as they operate in a similar manner. Different arrangements of arc-shaped ribs were used in these investigations. The researchers employed continuous arc-shaped parallel wires and observed a significant increments in Nusselt number and friction coefficient attributed to roughness [62],[63]. The optimal parameters were found to correspond to e/d ranged 0.0422 -0.426. At these parameters, friction coefficient and Nusselt number increased by factors of 1.75 and 3.80, in order, compared to smooth duct [62]. maximum THPP recorded was 1.7 [64], [65].

Maximum thermal efficiency was determined to be 79.84 % [64], and an enhanced exergy efficiency of 56% was reported [65].The effect of introducing a gap with a width equal to the roughness height in the continuous arc rib arrangement on structure of fluid flow and heat transmission was studied. The results indicated that the proposed roughness arrangement could lead to a further increment in Nusselt number with a lesser increment in friction coefficient compared continuous arrangement. Maximum THPP reached 1.94, compared to the value of 1.7 for the continuous arc ribs. Furthermore, the researchers demonstrated that the placement of a staggered rib part matching a relative size r/g of 4 resulted in an additional increase in the max. THPP, achieving a value of 2.27 [66],[67].

Authors in another study were utilized multi arc-shaped ribs and stated that max. THPP could be increased to 3.4 when optimal roughness parameters were employed [68]. The best results were obtained with W/w equal to 5. Also investigated multiple arc-shaped, centrally gapped roughness elements to enhance THPP of SAH. The findings revealed that the maximum THPP reached as high as 3.6, with roughness parameters of p/e = 8 [69],[70].

Likewise investigated the impact of adding a metal mesh as a roughness element on heat transmission and friction factor magnitudes. Experiments revealed that the maximum Nusselt number and friction factor were found 4 and 5 times higher, respectively, than smooth absorber plate. Maximum Nusselt number and friction coefficient obtained at L/e close to 47 and 72 respectively [71].

In their experiments, authors utilized an absorber plate with repeated transverse chamfered rib elements. The results showed that adding roughness geometry made the friction factor and Stanton number triple and double within the range of the studied parameters. Maximum Stanton number value was matching Reynolds number of 25 [72].

Authors examined the fluid structure and heat transmission improvement of SAHs arranged with traverse wedge-shaped rib featuring roughness. Their findings indicated that Nu number for the roughened plate was higher than that related value to the smooth duct by more than 2 times, while the friction factor showed even greater increase, reaching more than 5 times. Max. improvement in h was noticed at a wedge angle of approximately 10^o [73]. Regarding another study, authors investigated the effect of rib-groove roughness on flow dynamics and transmission of heat in SAH. Results indicated that the transferred heat rate was improved significantly with a minor increment in friction factors, compared to the configuration without groove. Max increase in friction coefficient and Nu number were noticed at 3.6 and 2.7 times, respectively, in comparison to smooth duct, obtained at a relative groove position of 0.4 [74].

In a different study, the authors used metal grit ribs with a staggered, circular cross section roughness arrangement in a SAH duct and experimentally tested the fluid characteristics and the heat transmission. Findings discovered that the transferred heat could be improved by up to 187% compared to smooth plate, but with a nearly 213% increase in the friction coefficient. Optimal heat transfer performance has been attained at P/e = 17.5. Whereas maximum friction coefficient was noted in a case with similar parameters at p/e = 12.5 [75]. Moreover, experimental evaluation of the thermal performance enhancement in a SAH due to the use of dimple-shaped elements roughness was conducted. The results indicated that the optimal heat transfer was achieved at p/e = 10, and the max, friction factor value was reported on the same p/e. Max friction coefficient and Nu number increased by more than 4 times and about two and half times, respectively, compared to a smooth duct [76].

A review of previous experimental and numerical studies on enhancing flow measurements and heat transmission in SAH through artificial roughness usage has been given in this chapter. Various roughness geometries are discussed, with a particular focus on investigations involving V-shaped ribs. It is well understood that heat transfer of SAH can be improved by utilizing artificial roughness on the heater plate, while, this application will increase the friction losses within the SAH duct. The literature highlights that V-shaped patterns, both in single and multiple arrangements, provide better THPP compared to the other types of artificial roughness. It was revealed that there is agitated mixing between primary air flow and the relatively strong secondary air flows produced by V-shaped ribs, thereby increasing the convective h near heater plate. However, the turbulent mixing can lead to increased pumping power requirements to maintain flow. Several investigations have aimed at optimizing the flow conditions and roughness parameters, and the Reynolds number, to identify the optimal parameters for maximizing THPP.

Furthermore, it was reported that gapped ribs can further enhance heat transfer rates more than the ungapped peers. In such cases, the main flow mixes with the subsidiary flow along the ribs, and entice turbulence through the gap, leading to stronger and turbulent mixing in the gap's downstream, therefor increasing the heat transfer rate. Various investigations have optimized the relative gap width and position to obtain the best thermal and hydraulic performance. Researchers have also explored the effects of placing staggered ribs at a distance from the gap on flow characteristics and heat transfer. The staggered ribs can disrupt and separate the flow emerging from the gap, causing vortices formation on either side of staggered ribs, with a more effective mix with the primary flow, thereby achieving further improvements in heat transfer rate. However, it was obvious that this may cause a simultaneous increase in friction losses. Consequently, many investigations have aimed to determine the optimal values for parameters affecting this matter, particularly staggered pitch length and staggered width, to achieve the best performance.

Despite the extensive studies on V-shaped ribs and their effectiveness on absorber plates, the subject still requires further investigations to be fully resolved. Much of the existing research has been experimental, focusing primarily on Nusselt number, friction factor, and THPP data. Numerical investigations using CFD software can provide detailed insights into flow structures, including secondary flows and regions of separation and reattachment. Furthermore, Kumar and Kim [49] found that employing a V-pattern rib combined with grooves provided better thermal performance compared to other V-ribs arrangement.

However, very few studies have examined this specific V-ribs arrangement or worked to determine the optimal groove shape for achieving maximum thermo-hydraulic performance. The existing study focusing conducting a comprehensive three-dimensional numerical investigation into fluid dynamics and heat transmission enhancement in a SAH plate, utilizing discrete V-shaped ribs with combined grooves of various shapes, specifically triangular, semi-circular, and trapezoidal. The analysis will be conducted using ANSYS Fluent software.

3. METHODOLOGY

3.1 COMPUTATIONAL FLUID DYNAMICS

Experimental procedures were widely executed to acquire heat transfer and fluid dynamics measurements in various engineering applications for many years. However, these procedures usually cost a lot of money and consume a significant amount of time. Furthermore, experimental tools and instrumentation cannot always provide detailed measurement for some practical problems and quantities, particularly in turbulent flow cases.

Computational Fluid Dynamics (CFD) tool has recently become very popular as an alternative for solving the complex governing equations of flow measurements and heat transmission in a wide range of engineering problems. Thanks to the recent astonishing progress in computer technology, it is now possible to numerically solve and analyses even difficult and challenging engineering problems and provide detailed information about the system. Nevertheless, CFD solutions are approximate and may introduce some errors, particularly in problems involving turbulent flow conditions. Successful use of CFD packages requires an understanding of all possible sources of error and the methods that can be employed to reduce them. Validating numerical data by comparing it against experimental or analytical results is always necessary to ensure reliable outcomes [77].

The CFD procedure includes defining a proper computational domain and then dividing it into a large number of structured or unstructured sub-domains or cells of different shapes and sizes, in a process called meshing. The parameters of the problem being solved, such as pressure, velocity, and temperature are then stored at the centers and/or corners of each cell in the mesh. The next step involves converting the partial differential equations that govern the performance of fluid flow and heat transmission into a set of equations which link the flow parameters stored neighboring cells, in a process called discretization. This approximation can be performed utilizing various approaches, the most common of which are Finite Volume (FV) and Finite Element (FE) methods. The final step in the numerical procedure is to solve the resulting discretized algebraic equations using one of the solution techniques, typically in an iterative fashion. This step results in a large set of data, which can be processed, analyzed, and presented in different forms [77],[78].

There are several commercial and in-house programmed CFD packages available for numerical simulation. One of the most widely used packages is ANSYS Fluent, which is employed in the current study. ANSYS fluent codes utilize the FV method for discretizing the equations that govern heat transmission and flow dynamics. This method starts with the integral forms of conservation equations, which are used in each Control Volume (CV) in the mesh. The integrals are then approximated, and the discretization process is conducted to produce a system of algebraic equations. This method has various advantages over other discretization methods, including the ability to handle complex unstructured meshes, making it applicable to complicated geometries. Additionally, it is conservative by nature, for each CV and for the entire computational domain [79],[80] .

3.2 GOVERNING EQUATIONS

Present study includes a three-dimension simulation of internal duct fluid flow and heat transfer, using ANSYS Fluent software governing equations to solve the problem are Reynolds Averaged Naiver Stocks (RANS) and energy equations. For steady-state, incompressible, turbulent flows, these equations are defined in tensor form by the following relations [81].

a. Continuity equation

$$\frac{\partial\left(\rho U_j\right)}{\partial x_j} = 0 \tag{3.1}$$

b. Momentum equations

$$\frac{\partial\left(\rho U_i U_j\right)}{\partial x_j} = -\frac{\partial P}{\partial x_i} + \frac{\partial}{\partial x_j}\left[\mu\left(\frac{\partial U_i}{\partial x_j} + \frac{\partial U_j}{\partial x_i}\right) - \rho\overline{u_i' u_j'}\right] \tag{3.2}$$

c. Energy Equation

$$\frac{\partial\left(\rho U_j T\right)}{\partial x_j} = \frac{\partial}{\partial x_j}\left(\frac{\mu}{Pr}\frac{\partial T}{\partial x_j} - \rho\overline{u_j' T'}\right) \tag{3.3}$$

All symbols in the above equations have their usual meanings, with the prime symbol denoting the fluctuation part of the quantity. These turbulence terms, specifically the Reynolds stresses ($-\rho\overline{u_i'u_j'}$) and the turbulent heat flux ($-\rho\overline{u_j'T'}$), are additional unknows and need to be modelled to mathematically close the set of equations (3.1 to 3.3); this process is referred to as turbulence modelling. The appropriate selection of the turbulence model is a critical step to ensure the numerical solution is accurate. The most common approach belongs to the Eddy Viscosity Models (EVMs) group, which uses the Boussinesq approximation to model the turbulence quantities. According to EVMs, the turbulent heat flux and Reynolds stresses are modelled using the equations [82],[83] :

$$-\rho\overline{u_i'u_j'} = \mu_t\left(\frac{\partial U_i}{\partial x_j} + \frac{\partial U_j}{\partial x_i}\right) - (2/3)\rho k\delta_{ij} \tag{3.4}$$

$$-\rho\overline{u_i'T'} = (\mu_t/\sigma_t)\frac{\partial T}{\partial x_i} \tag{3.5}$$

where k, μ_t and σ_t are the kinetic energy, viscosity, and Prandtl number of turbulences. The turbulent viscosity can be modelled using one of the various available turbulence models, in most cases, one of the two-equations models is used. Based on recommendations from previous work, the RNG (Re-Normalized Group) kinetic energy – dissipation ($k - \varepsilon$) model is employed in the current study. RNG $k - \varepsilon$ model is similar to the standard $k - \varepsilon$ model, with some refinements that make it more exact and consistent for a wide range of flow characteristics [77].Turbulent viscosity in this model is defined by the equation

$$\mu_t = \rho C_\mu k^2/\varepsilon \tag{3.6}$$

where C_μ Constant= 0.0845, while k and ε are obtained using the transport equations [77]

$$\frac{\partial(\rho k U_i)}{\partial x_i} = \frac{\partial}{\partial x_j}\left(\alpha_k\mu_{eff}\frac{\partial k}{\partial x_j}\right) + G_k + G_b - \rho\varepsilon + S_k \tag{3.7}$$

$$\frac{D(\rho\varepsilon U_i)}{Dt} = \frac{\partial}{\partial x_j}\left(\alpha_\varepsilon\mu_{eff}\frac{\partial\varepsilon}{\partial x_j}\right) + C_{\varepsilon1}\frac{\varepsilon}{k}(G_k + C_{\varepsilon3}G_b) - C_{\varepsilon2}\rho\frac{\varepsilon^2}{k} - R_\varepsilon + S_\varepsilon \tag{3.8}$$

where G_k and G_b represent the generation of turbulent kinetic energy due to the mean velocity gradient and buoyancy, respectively, and they defined by the expressions: $G_k = -\rho\overline{u_i' u_j'}\,\partial U_i/\partial x_j$, $G_b = -g_i(\mu_t/\rho\sigma_t)\,\partial\rho/\partial x_i$; μ_{eff} represents the effective viscosity; α_k and α_ε are the inverse effective Prandtl numbers for k and ε, respectively; S_k and $S_\varepsilon$are source terms defined by user. The R_ε term in the ε equation is given by $R_\varepsilon = [C_\mu\rho\eta^3\,(1-\eta/\eta_0)/(1+\beta\eta^3)](\varepsilon^2/k)$, where $\eta = Sk/\varepsilon$ (S is strain tensor mean rate), $\eta_0 = 4.38$, and $\beta = 0.012$. The model constants are $C_{\varepsilon 1} = 1.42$ and $C_{\varepsilon 2} = 1.68$.

3.3 THPP ANALYSIS

To evaluate the effectiveness of a SAH system, thermal and hydraulic performances analysis must be performed. The SAH's thermal efficiency is defined by equation:

$$\eta_{th} = \frac{Q_u}{Q_c} \tag{3.9}$$

where Q_u and Q_c are the flowing air useful heat and the solar radiation heat incident on the SAH duct, respectively. These quantities are defined by the following expressions:

$$Q_u = \dot{m}C_p(T_o - T_i) = hA_s(T_w - T_b) \tag{3.10}$$

$$Q_c = IA_s \tag{3.11}$$

In these equations, $\dot{m}$ is air mass flow rate, C_p is air specific heat, T_o and T_i are the outlet and inlet air temperatures, respectively, T_w the temperature of the absorber plate, T_b is the bulk fluid temperature defined as $T_b = (T_i + T_o)/2$, , A_s is heater plate area, h is convective heat coefficient and I is the solar radiation intensity. Air mass flow rate is obtained from :

$$\dot{m} = \rho V A_c = \rho VWH \tag{3.12}$$

where V air velocity A_c duct cross section area.

Reynolds number is defined by equation:

$$Re = \frac{\rho V D_h}{\mu} \tag{3.13}$$

where ρ, μ are the density and air dynamic viscosity, respectively, and D_h is duct hydraulic diameter, defined as $D_h = 4WH/2(W + H)$.

The Nusselt number is expressed as:

$$Nu = \frac{hD_h}{k} \tag{3.14}$$

k is air thermal conductivity. h can be evaluated using the expression derived from equation (3.10):

$$h = \frac{Q_u}{A_s(T_w - T_b)} \tag{3.15}$$

Airflow through the duct encounters friction losses, which can be represented by the friction factor defined in the equation:

$$f = \frac{(\Delta P/L)D_h}{2\rho V^2} \tag{3.16}$$

ΔP is pressure drop across duct and L is duct length.

The overall performance of a roughened duct is determined by considering both thermal and hydraulic performances. While the heat transfer rate is enhanced by artificial roughness, it simultaneously increases the pressure drop across the duct. THPP is introduced to express the overall performance of roughened surfaces. It is defined by the equation:

$$THPP = \frac{Nu/Nu_s}{(f/f_s)^{1/3}} \tag{3.17}$$

where Nu, f and Nu_s, f_s are Nusselt numbers and friction factors for roughened and smooth duct, respectively.

3.4 CASE STUDY AND METHODOLOGY

This study includes a detailed three-dimensional numerical investigation of heat transmission enhancement and fluid flow structure in SAH featuring an absorber plate with V-shaped ribbed artificial roughness elements. The simulation is conducted using ANSYS Fluent 19 commercial software. The analysis focuses primarily on determining the effects of roughness configuration and parameters on Nusselt numbers, friction factors, and THPP values for Reynolds numbers varying from 3000 to 15,000. Detailed results and discussions will be presented in Chapter Four. Furthermore, a validation case against relevant experimental data available in literature is carried out prior to the main simulations to increase confidence in the numerical results obtained later. The validation data and the methodology framework of the numerical simulation using ANSYS fluent program are presented in the following sections. The steps followed are explained using the SAH model employed in the validation study, which is identical to that experimentally investigated in [34].

3.4.1 Geometry and Computational Domain

The study geometry, which is a SAH duct with continuous V-down ribs on its wide wall, is modeled as a control volume within the ANSYS program environment, as illustrated in Figure 3.1. The duct dimensions are 1400 × 300 × 25 mm for length, width, and height, respectively, resulting in an aspect ratio (AR) of 12 and a hydraulic diameter (D_h) of 4.6 cm. The ribs height (e) is 2 mm, P is 20 mm, and α =º60. The duct, roughness, and flow specifications are listed in table 3.1. The computational domain includes sections of entry and exit to ensure flow is fully developed and end effects are minimal. All specifications are identical to those in the study by [34] which is utilized in the validation case.

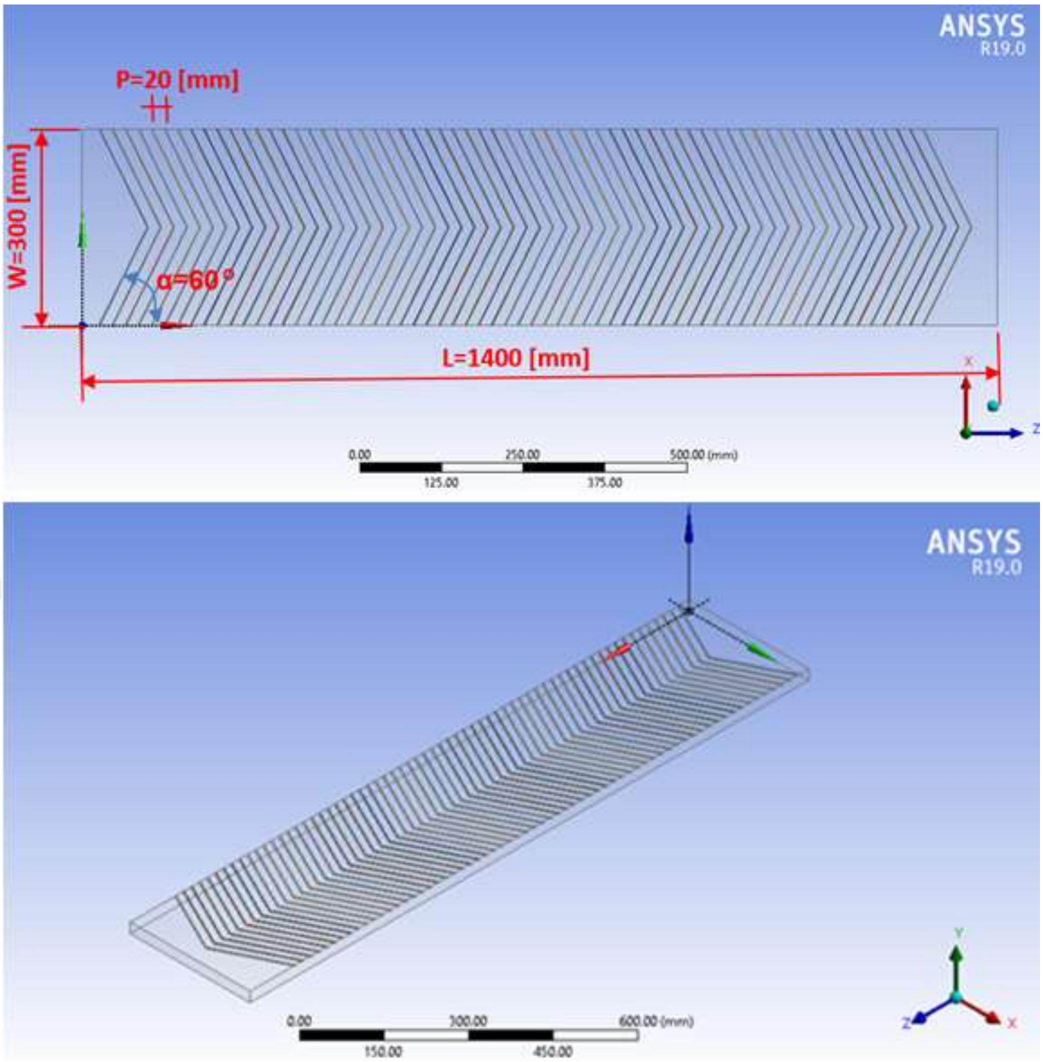

Figure 3.1: The SAH Geometrical Model -the Computational Domain.

Table 3.1: Duct, Roughness, and Flow Parameters Values.

Parameter	**Value**
AR	12
P/e	10
e/D_h	0.043
α	°60
Re	$3*10^3 – 15*10^3$

3.4.2 Generation of Mesh

Mesh is constructed using the ANSYS Fluent program, utilizing unstructured control volumes and employing face seizing with a cell size of 5 mm on each wall of the computational domain. An inflation layer is applied at common surface interfaces with a growth rate of 1.2, a transmission factor of 0.272, and five layers to accurately depict the occurring changes. A mesh sensitivity analysis is applied to make sure of mesh-independent solutions. Various meshes configurations of increasing refinements are examined to obtain accurate and economical numerical solutions. Figure 3.2 demonstrates how Nusselt number is varying depending on the element numbers for seven meshes at a Re $=15*10^3$ It is obviously noticed that the sixth mesh provides a proper choice, as further refinement does not significantly affect the accuracy of the results. Therefore, the specifications of this mesh are adopted in the present study. Figure 3.3 illustrates a detailed view of the selected mesh used for discretizing the computational domain as described above. The total number of elements and nodes is 823,668 and 168,438, respectively.

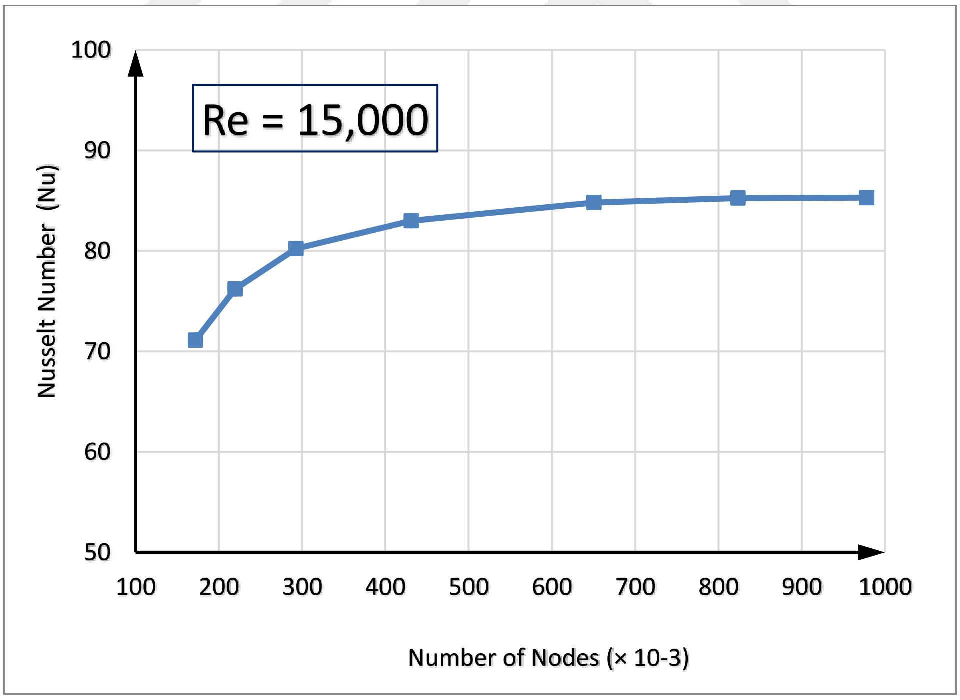

Figure 3.2: Grid Independence Test.

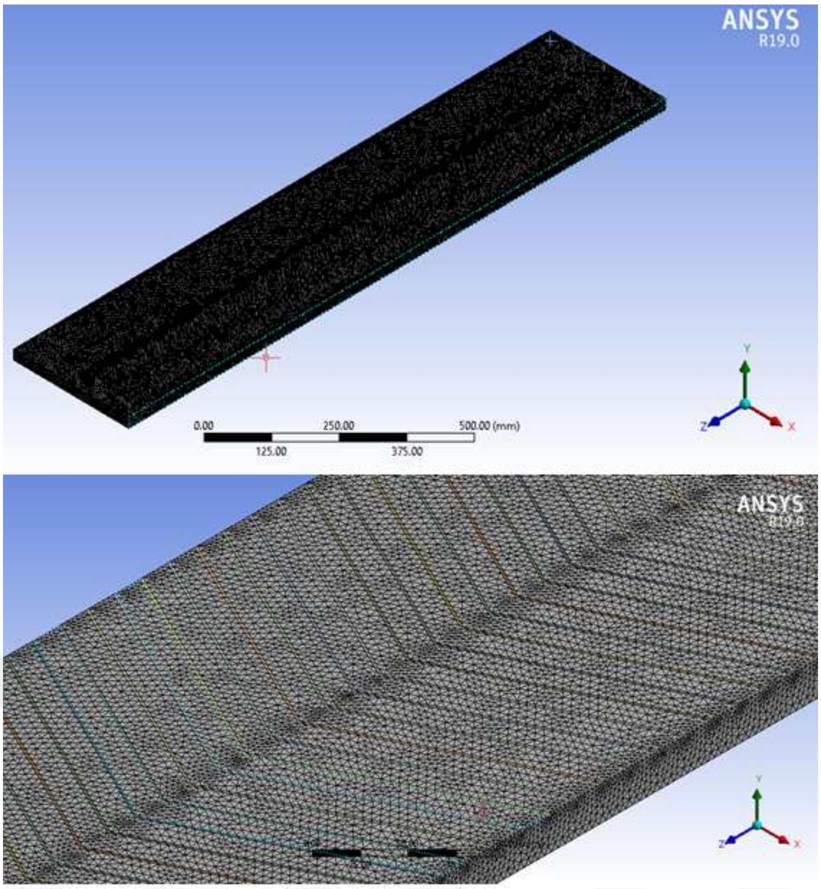

Figure 3.3: Computational Domain's Mesh**.**

3.4.3 Boundary Conditions

Figure 3.4 illustrates the boundary surfaces of the computational domain, while table 3.2 presents the detailed values of the applied boundary conditions. At the inlet, temperature and velocities corresponding to the examined Reynold numbers are specified, while a standard pressure value is set at the outlet. A constant heat flux is considered to the upper ribbed heater plate, in the meantime, other duct walls are considered as adiabatic.

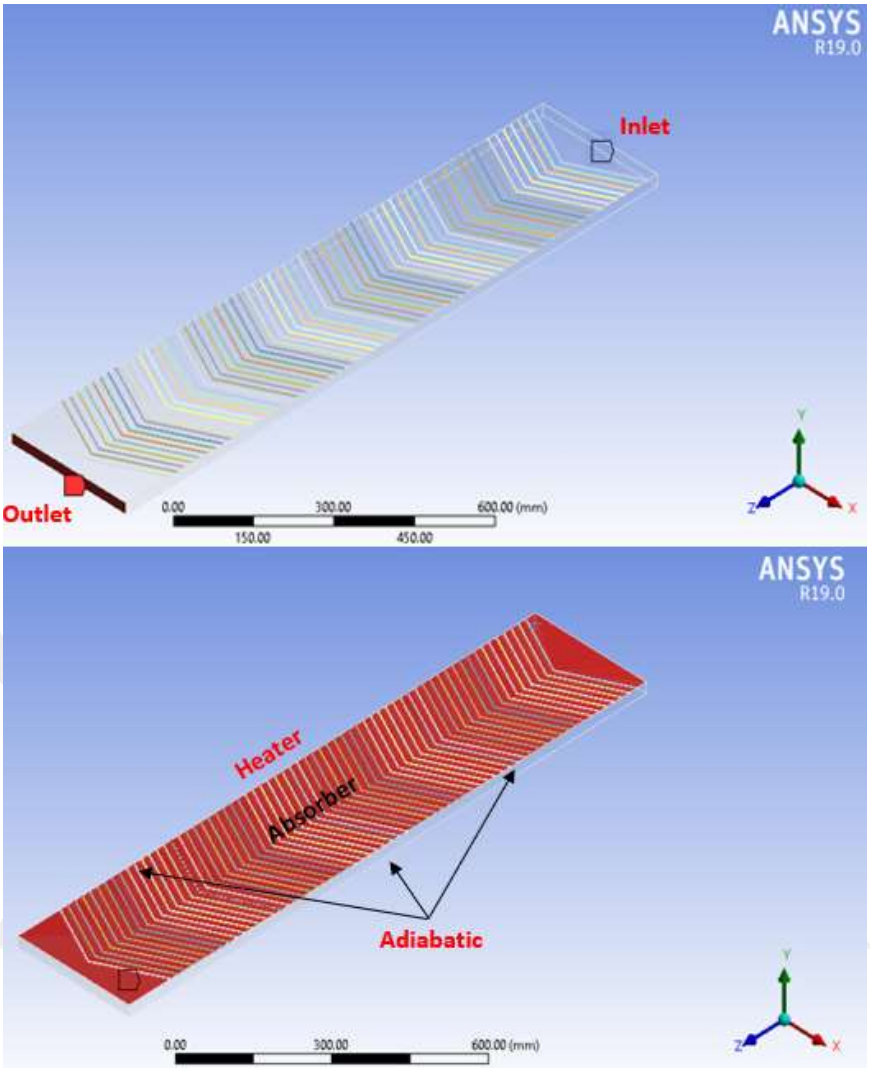

Figure 3.4: The surface Names and Boundary Conditions.

Table 3.2: Boundary Conditions Imposed on the Computational Domain.

Boundary	**Type**
Inlet	T_{in}= 19.5 ºC Re = 3000, 6000, 9000, 12,000, 15,000
Outlet	Standard pressure
Heated surface	Heat flux = 1000 W/m^2
Side and bottom walls	Adiabatic

3.4.4 Numerical Settings

The airflow in the duct is assumed steady state, three dimensional, and fully developed turbulent flow. Turbulence modelled using RNG k-ε to enclose the governing equations. FV method was utilized to discretize the partial differential equations with a first order backward difference scheme. Semi Implicit Method for Pressure Linked Equation (SIMPLE) is utilized to couple velocity and pressure fields. The energy model uses a segregated temperature approach with second-order accuracy. The air model is considered ideal, and the gravity and buoyancy effects are included. The convergence condition for all equations being solved are set to no less than 10^{-3}.

3.4.5 Results Validation

The current study numerical model and settings validation was confirmed by comparing the simulation data with the experimental research presented by authors in [34],who investigated a SAH with identical specifications. This comparison includes both Nu number and friction coefficient values for Re numbers of $3*10^3$, 6000, 9000, 12,000 and 15,000. This validation procedure is considered critical in simulations using commercial software that numerically solve the Reynolds-Averaged Navier Stocks (RANS) equations, such as ANSYS Fluent.

Figures 3.5 and 3.6 demonstrate the comparison results. It is evident from these figures that the present numerical outcome match to good extent with experimental data in reference. The maximum deviations observed, corresponding to the highest Re number case, are approximately 12% for the Nu number and 13% for friction factor. These relatively small deviations can be attributed to real-world conditions that are not included in the simulation. Nevertheless, the relative errors are still minor, confirming that ANSYS Fluent, when used with an appropriate turbulence model, can accurately predict the heat and fluid behavior within the ribbed SAH duct. Therefore, one can proceed to the forthcoming main numerical cases with a high level of confidence.

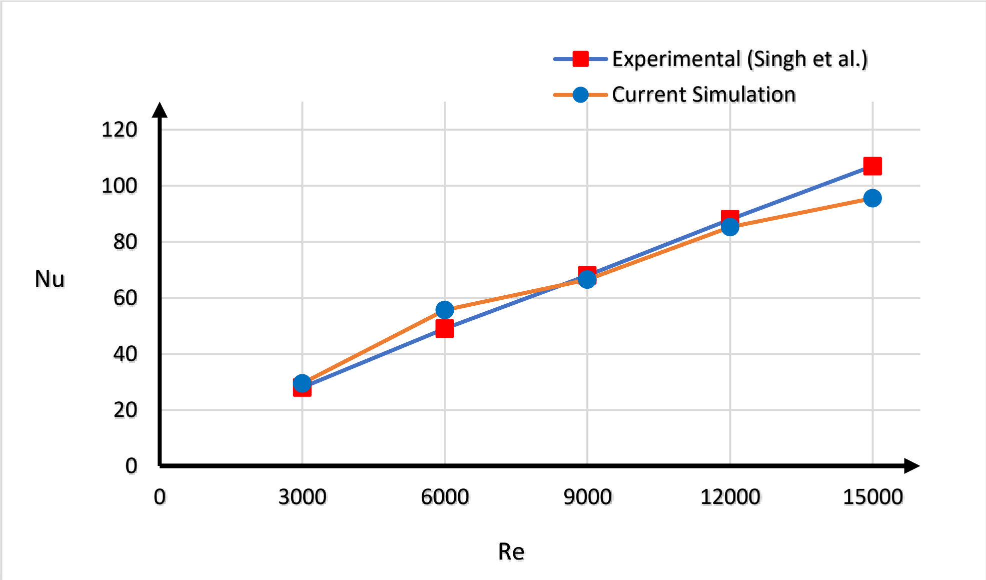

Figure 3.5: Nu number Comparison With Reference Experimental Results.

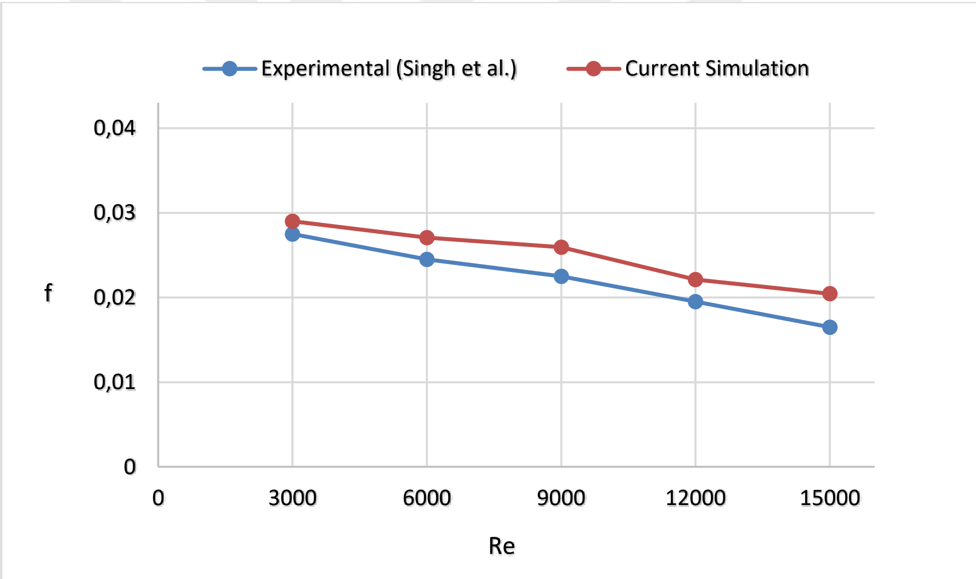

Figure 3.6: Friction Factor Comparison With Reference Experimental Results.

4. RESULTS AND DISCUSSIONS

Present study conducts a three-dimensional numerical investigation into the enhancement of heat transmission and flow measurements within SAH duct. This research utilizes a broken V-shaped ribs pattern combining grooves of various shapes, specifically triangular, semi-circular, and trapezoidal. The simulation was done using the ANSYS Fluent commercial software package. The analysis includes the determination of Nusselt numbers, friction factors, and THPP. Additionally, detailed flow counters are provided to highlight the various flow regions, further clarifying the results. The dimensions of the duct and the key artificial roughness parameters were selected based on optimal results from the literature, specifically the study by authors in [34],which was used in the validation study. The investigation is carried out for Re number was varied from $3*10^3$ to $15*10^3$. The simulation analysis begins by examining a duct roughened plate with broken V-shaped ribs without grooves, and then progresses to cases incorporating grooves to demonstrate the effects of the new roughness configuration.

4.1 BROKEN RIBS WITHOUT GROOVES

Figures 4.1 and 4.2 illustrates both 3D and 2D views of the SAH duct considered in the current study, highlighting the roughened absorber plate and defining the duct and roughness parameters, with a focus on the gaps in the ribs. The duct dimensions are as follows: the length (L) is 1400 mm, the width (W) is 0.3 m, and height (H) is 0.025 m, resulting in a AR of 12, and Dh of 46 mm. The absorber plate is roughened using discrete V-down ribs applied to its underside. e is 2 mm, P is 16 mm, α is o60, and the gaps position (d) and width (g) are 97.5 mm and 2 mm, respectively. These specifications for the roughness geometry are selected identical to those of the optimal corresponding case presented in [34]. Table 4.1 provides the key duct and relative roughness parameters. A constant heat flux of 1000 W/m2 is applied to the upper ribbed absorber plate, while the remaining walls of the duct are kept insulated. Air enters the roughened duct at an inlet temperature of 19.5 oC and standard pressure, flowing at rates corresponding to Re numbers of 3000, 6000, 9000, 12,000, and 15,000. The heat transfer and fluid flow data for this case are present and discussed in the following sections.

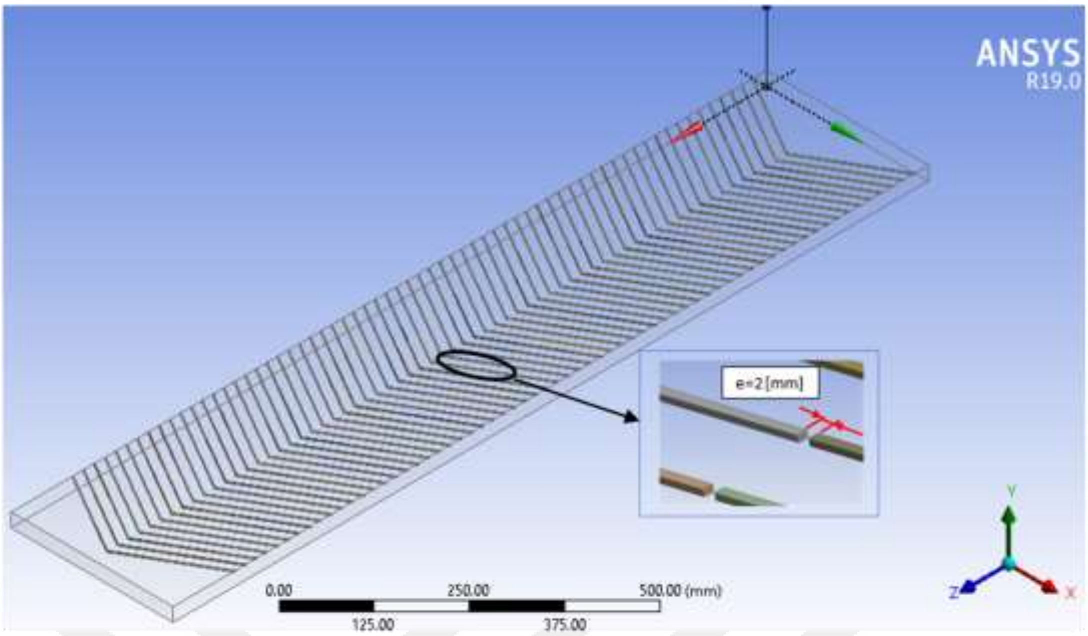

Figure 4.1: The SAH Geometrical Model- 3D View.

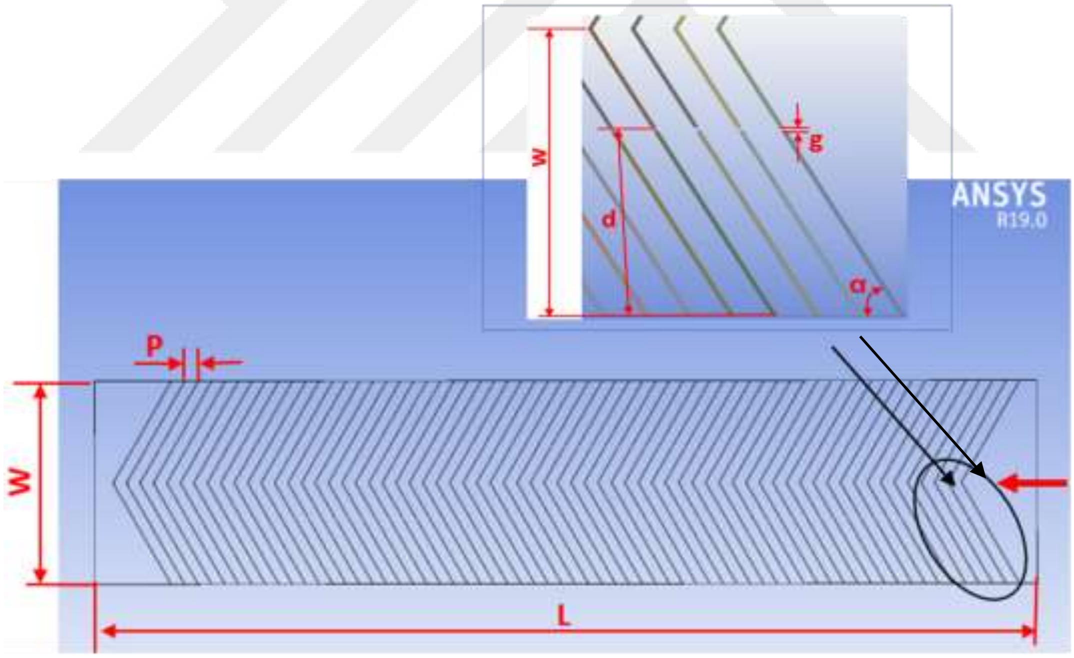

Figure 4.2: The SAH Geometrical Model - 2D View With Naming Key Duct and Roughness Parameter.

Table 4.1: Duct Roughness Parameters Values.

Parameter	Value
AR	12
α	º60
e/D	0.043
P/e	8
d/W	0.65
g/e	1

4.1.1 Heat Transfer Analysis

Figure 4.3 demonstrates that Nu number at different Re number for the roughened SAH. The figure also presents the experimental variations reported by authors in [42]. For further validation of the numerical results. Additionally, data for a smoot plate and for the continuous V-shaped ribs obtained previously are also included for comparison purposes. The Nu numbers for a smooth plate are calculated using Dittus-Boelter equation specified by [84]:

$$Nu = 0.023Re^{0.8}Pr^{0.4} \tag{4.1}$$

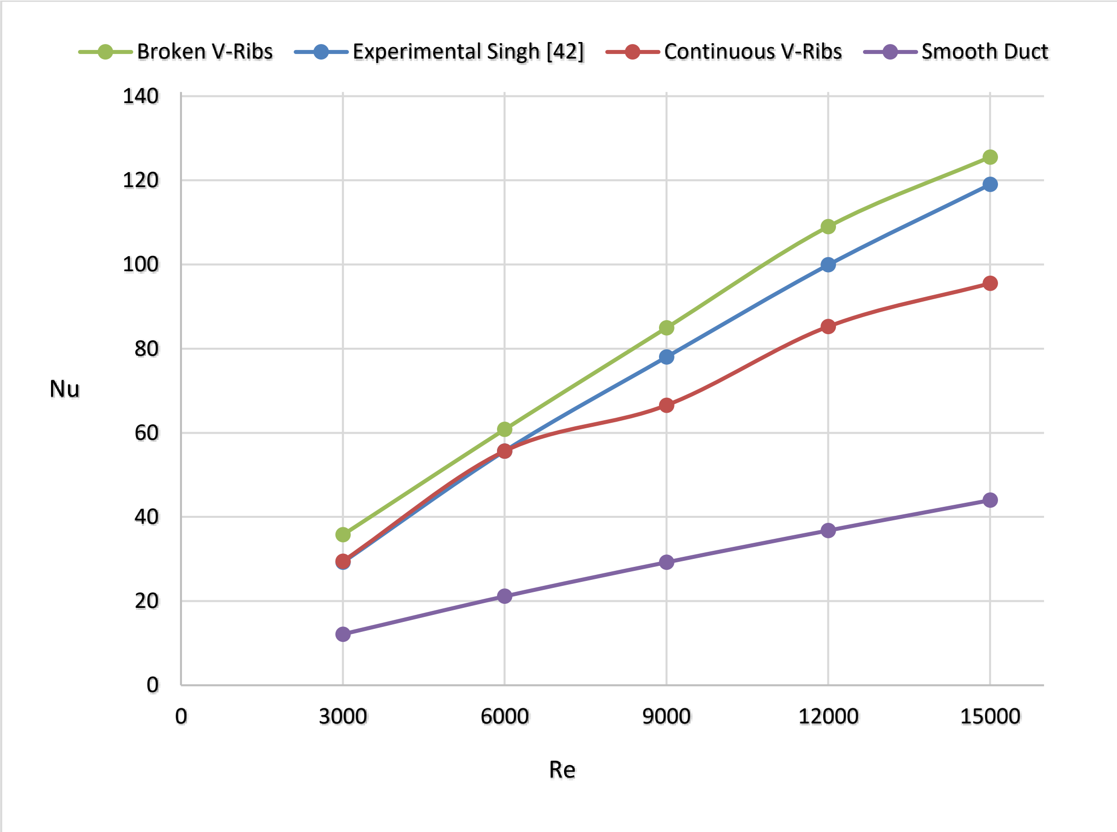

Figure 4.3: Nu Number Change With the Re Number for Broken V-shaped, Continuous V-shaped Ribbed Ducts, and Smooth Ducts.

The results indicate that increasing Re numbers lead to a significant increment in Nu number values across all cases. This was due to the augmented turbulence levels resulting from higher Re numbers. This behaviour is more pronounced in the situation of broken V-shaped ribs compared to continuous V-shaped ribs, due to the increased velocity of flow downstream of gaps. The deviation between discrete and continuous ribs becomes more significant at higher Re number values. For example, the Nu number increased from 35.7 at a Reynolds number of 3000 to 125.5 at a Reynolds number of 15,000 for the broken V-ribs. The corresponding increases for the continuous V-ribs were from 29.5 at a Reynolds number of 3000 to 95.5 at a Reynolds number of 15,000.

The results can be further explained by examining the velocity vectors contours for ducts with continuous and discrete V-ribs, as illustrated in figures 4.4 and 4.5. It can be observed that the increased velocity magnitude and enhanced mixing levels of the secondary and main flows downstream of the gaps may reduce the regions of low heat transfer rates upstream of the ribs, consequently increasing the Nusselt numbers.

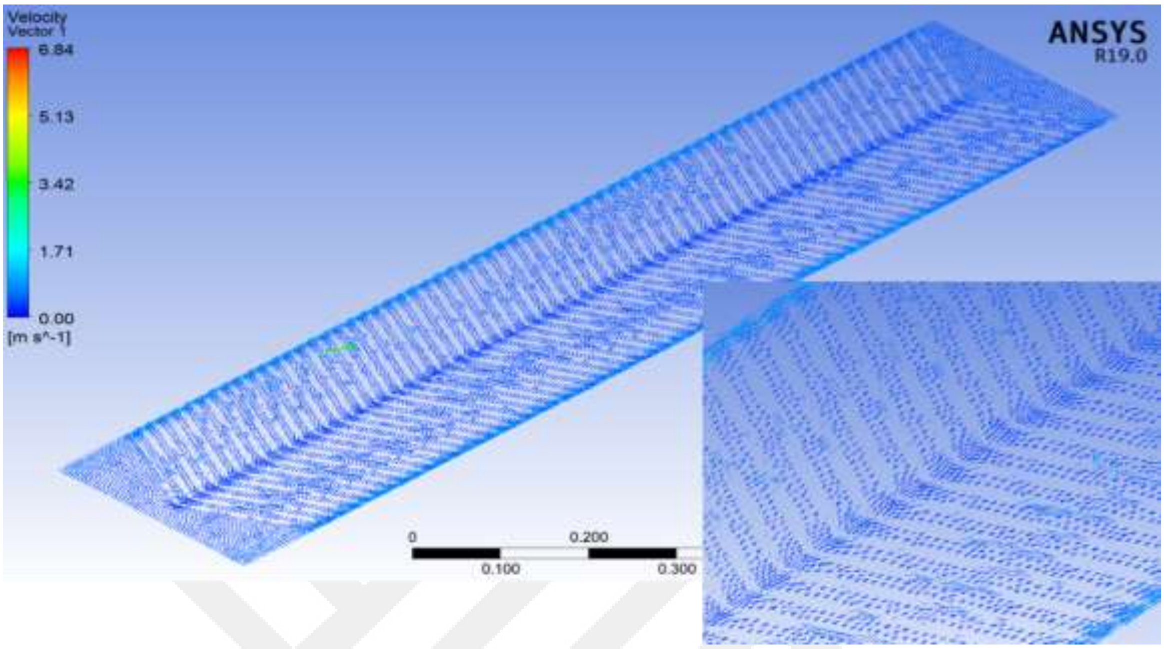

Figure 4.4: Velocity Vector for a Continuous V-shaped Ribbed Duct at Re = 9000.

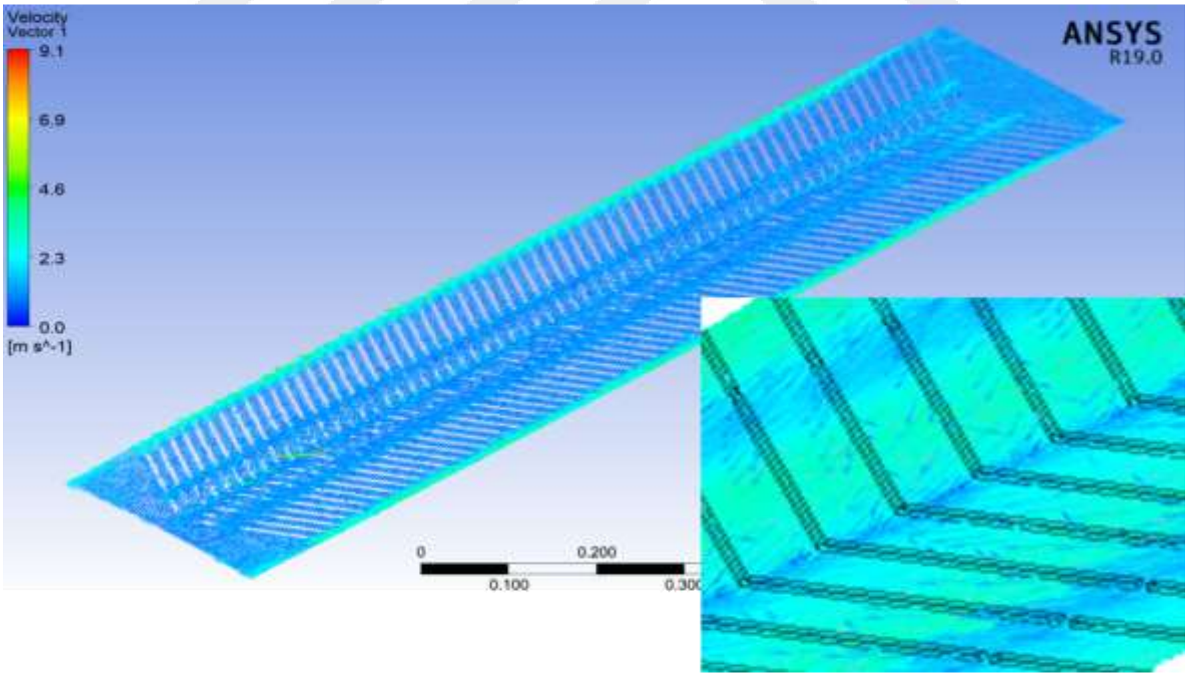

Figure 4.5: Velocity Vector for Broken V-shaped Ribbed Duct at Re= 9000

Furthermore, figure 4.3 demonstrates that the enhancement in Nusselt number for discreate and continuous V-shaped roughness compared to a basic smooth duct shows that the maximum increase in Nusselt numbers reaches approximately 3 times and 2.2 times that of a smooth duct, for the discrete and continuous configurations, respectively. In other words, applying gaps in the V-shaped ribs can improve Nu number by up to 30% compared to the related continuous arrangement. Finally, regarding the comparison between the current numerical data and the experimental findings reported by authors in [42] for similar duct and roughness shapes and parameters, the figure shows a good match between both set of results. The maximum deviation between the Nu number results does not exceed the value 8 % for all Reynolds numbers considered in this investigation. This provides further validation for the current numerical results.

4.1.2 Friction Analysis

In analyzing heat and fluid flow problems, it is crucial to determine the drop of pressure resulted from the flow. The power demand to drive the flow is directly related to friction losses, the matter of primary interest in many engineering applications. Figure 4.6 illustrates the variations in the average friction factor at different Re numbers for broken and discrete V-shaped roughened ducts. For validation purposes, reference experimental data provided in [42] is included. The current numerical data aligns closely with the reference experimental data, with a maximum deviation of no more than 9%. The figure also presents data for a smooth plate, calculated by Blasius modified equation [81], for comparison purposes.

$$f = 0.085Re^{-0.25} \tag{4.2}$$

Moreover, figure 4.6 indicates that both continuous and broken V-shaped ribbed ducts exhibit significantly higher friction factors compared to smooth plate. Max. increase in the friction coefficient in the roughened plates can reach up to three times greater than that of the smooth plates. Maximum increase in friction factors occurs at low Re numbers. In contrast to the data on Nusselt number, there is only a slight difference between the friction factor values for continuous and discrete V-ribs arrangements. The continuous arrangement shows slightly higher values at Reynolds numbers less than 9000, while the trend reverses at higher Reynolds numbers. This finding is consistent with the experimental observations reported in [42].

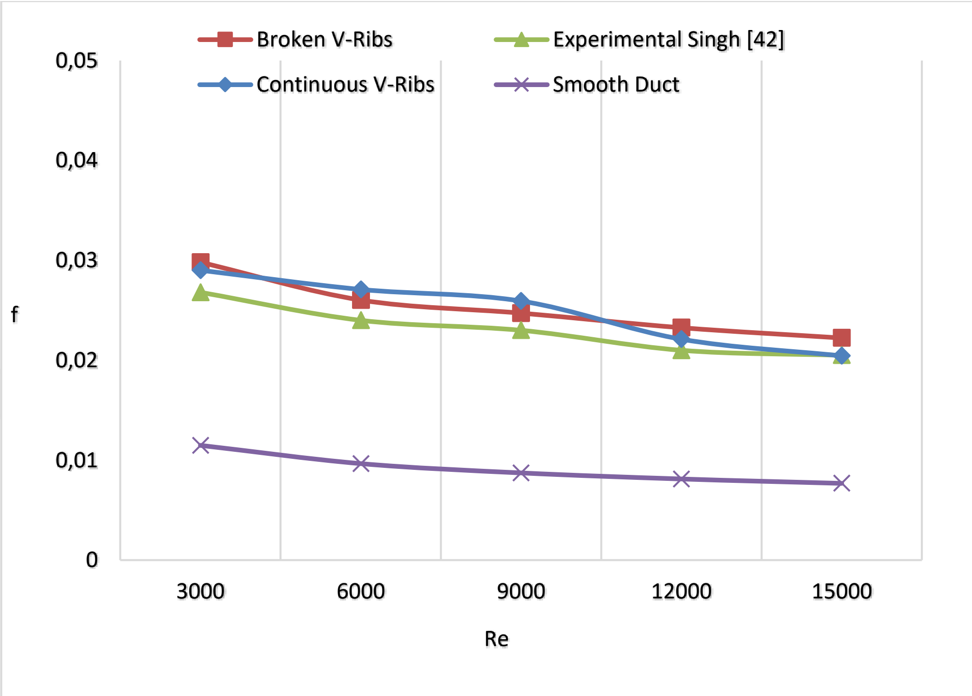

Figure 4.6: Friction Factor Variation with the Re for Broken V-shaped, Continuous V-shaped Ribbed Ducts, and Smooth Ducts.

The figure demonstrates that the friction factor inclines to decrease with the increasing number of Re for both smooth and roughened ducts. For smooth dust, this performance can be credited to the fact that by increasing Re number the inertial forces impact begins to dominate over the viscous forces' effects, leading to reduced resistance to flow. For ribbed duct, the situation is more complex, and the friction factor can be influenced by various factors, including roughness geometry, turbulence mixing, flow separation and reattachment, and secondary flow dynamics. Increasing Reynolds number, combined with the existing roughness elements, reduces the thickness of the viscus sublayer, hence diminishing viscous effects. Furthermore, higher Reynolds numbers lead to enhanced flow mixing and a reduction in drag forces, also leading to a decrease in the friction factor.

4.1.3 THPP

The results indicate, consistent with the literature, that employing artificial roughness can enhance heat transfer, while at the same time the pressure drop across the duct. Therefore, it is beneficial to calculate and present THPP to evaluate the overall performance of the roughness. This parameter, defined by equation 3.17, considers the impact of both heat transfer and friction losses.

Figure 4.7 demonstrates the THPP for ducts with discrete and continuous V-shaped roughness elements, at various Re. Results show that the THPP values exceed unity across all Reynolds number ranges considered in this study, indicating a positive effect of employing artificial roughness. It can be also noted that THPP values slightly varies with increasing Re number, particularly in status of discreate V-ribs. This means that the enhancement in the Nu number resulting from increasing Re number is offset by the simultaneous increase in friction factors.

Furthermore, figure 4.7 illustrates that the THPP's for broken ribs are greater than those in the case of continuous ribs. This observation corresponds with the finding that broken V-ribs result in a significant enhancement of Nusselt numbers with only a limited variation in friction factors compared to continuous ribs. The THPP values range from 2.0 to 2.15 for the discrete ribs case and from 1.57 to 1.87 for the continuous rib case. These values for the discrete V-shaped ribs are in excellent matching with the experimental values indicated in [43], who used a nearly identical roughened duct arrangement, and claimed that his values were superior in comparison to other roughness configurations stated in the literature.

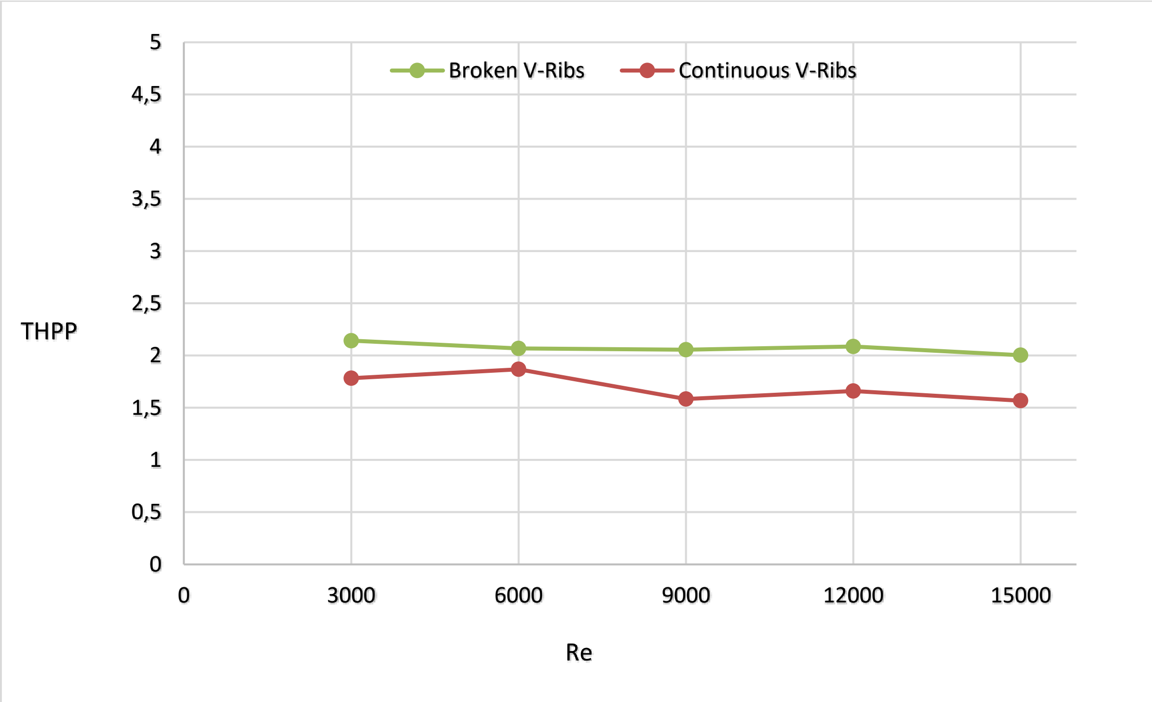

Figure 4.7: THPP Variation with the Re Number for Broken and Continuous V-shaped Ribbed Ducts.

4.2 COMBINED BROKEN V-SHAPED RIBS AND GROOVES

The effect of introducing grooves in the ribbed heater plate on heat and fluid flow behavior is also examined in this research. The dimensions of the duct and the parameters of the discrete V-shaped ribs are maintained similar to those used in the first part of the study. The boundary conditions and Reynolds number range are also maintained identical to the previous scenarios without grooves. The grooves are positioned in the mid distance between two successive ribs, maintaining a similar attack angle. Three different grooves cross-sections are considered in this investigation, specifically triangular, semi-circular and trapezoidal. The relative depth (h/e) of all grooves is set to unity, the apex angle of the triangular groove is specified to be o60, and the short base of the trapezoid is defined to be equal to half of the rib height i.e. 1 mm. Figure 4.8 illustrates the schematic of the roughened duct with details of the three shapes of the grooves, highlighting their key dimensions.

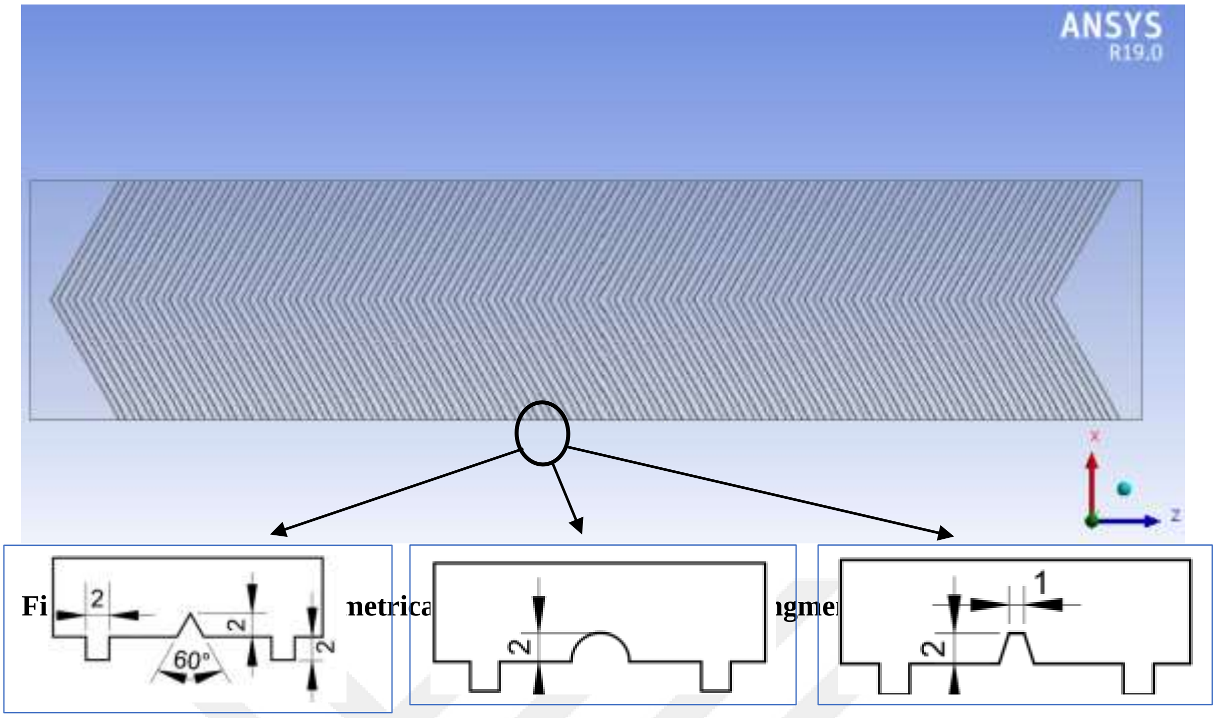

Figure 4.8: The SAH Geometrical Model – (rib-groove) Arrangement.

4.2.1 Heat Transfer Analysis

Figure 4.9 illustrates the variations of Nu with Re for roughened ducts featuring various arrangements, including broken V-shaped ribs and a combination of broken V-shaped ribs and grooves, with triangular, semi-circular, and trapezoidal shapes. The objective is to compare the effect of applying grooves of different shapes to the broken V-ribs configuration on heat transfer rates. The data of a smooth duct is also included for further comparison.

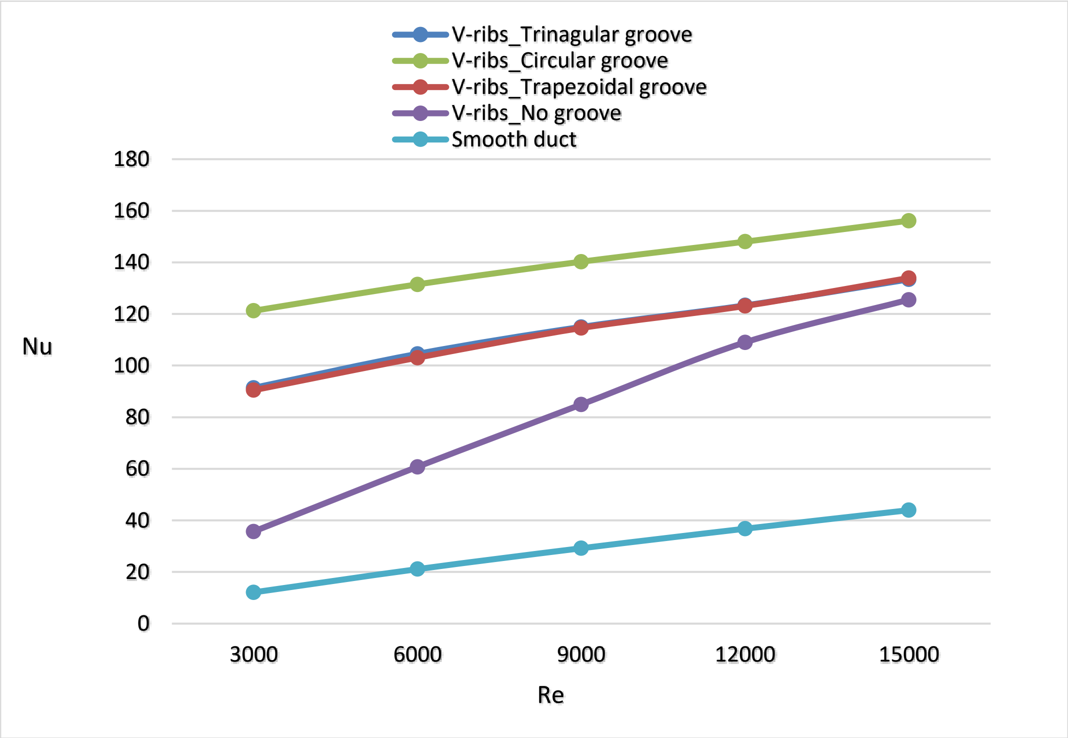

Figure 4.9: Nu Variation with Re for Roughened Ducts with Various Arrangements: Broken V-Shaped Ribs and Combined Broken V-Shaped Ribs and Grooves Of Triangular, Circular and Trapezoidal Shapes.

It can be observed from the figure that the Nu rises with increased Re number for all configurations examined in the study, due to the enhanced turbulence levels, as discussed previously. Regardless of the groove shape, introducing grooves to the discrete V-ribs causes a remarkable increase in heat transmission rates, with the circular groove showing a clear advantage over the other groove shapes. The maximum average Nusselt number for the semi-circular groove exceeds 156 at a Re number of 15,000, while the values for the triangular and trapezoidal grooves are almost identical at about 133. The Nusselt number values for the broken V-ribs arrangement without groove and for a plain duct are 125 and 44, respectively, at the same Reynolds number. This means that the enhancement in Nusselt number as a result of employing a semi-circular groove is 1.25 times that of a corresponding arrangement without groove and exceeds 3.5 times that of a smooth duct. The corresponding values for the cases with triangular and trapezoidal grooves are 1.06 and 3, respectively. The significant enhancement in heat transfer obtained in the V-ribs – groove pattern can be explained by the larger surface areas and enhanced turbulence intensity caused by induced vortices in this combination. A similar impact of groove creation was reported in [49] and [74], who studied heat transfer enhancement employing ribs-groove artificial roughness.

Temperature and velocity vectors contours can further explain the results obtained. Figure 4.10 demonstrates high temperature regions across ribs and grooves in spanwise direction, particularly in regions where the two subsidiary flows developed all the way of the ribs and grooves converge, and also in areas close to the gaps created across the ribs. Figure 4.11 illustrates the subsidiary flows and the accelerated flow through the gaps. The interaction between these subsidiary flows along the ribs and grooves and the main flow over ribs, in addition to the multiple detachment and reattachment of flow, significantly contributes to the heat transfer improvement.

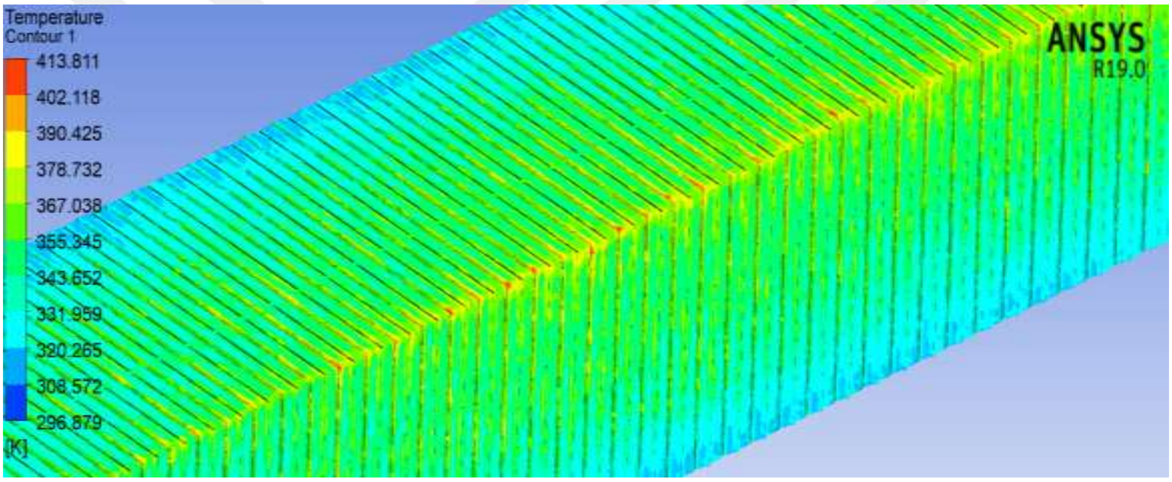

Figure 4.10: Temperature Contour for the Case of Discrete V-ribs With Circular Groove at Re=3000.

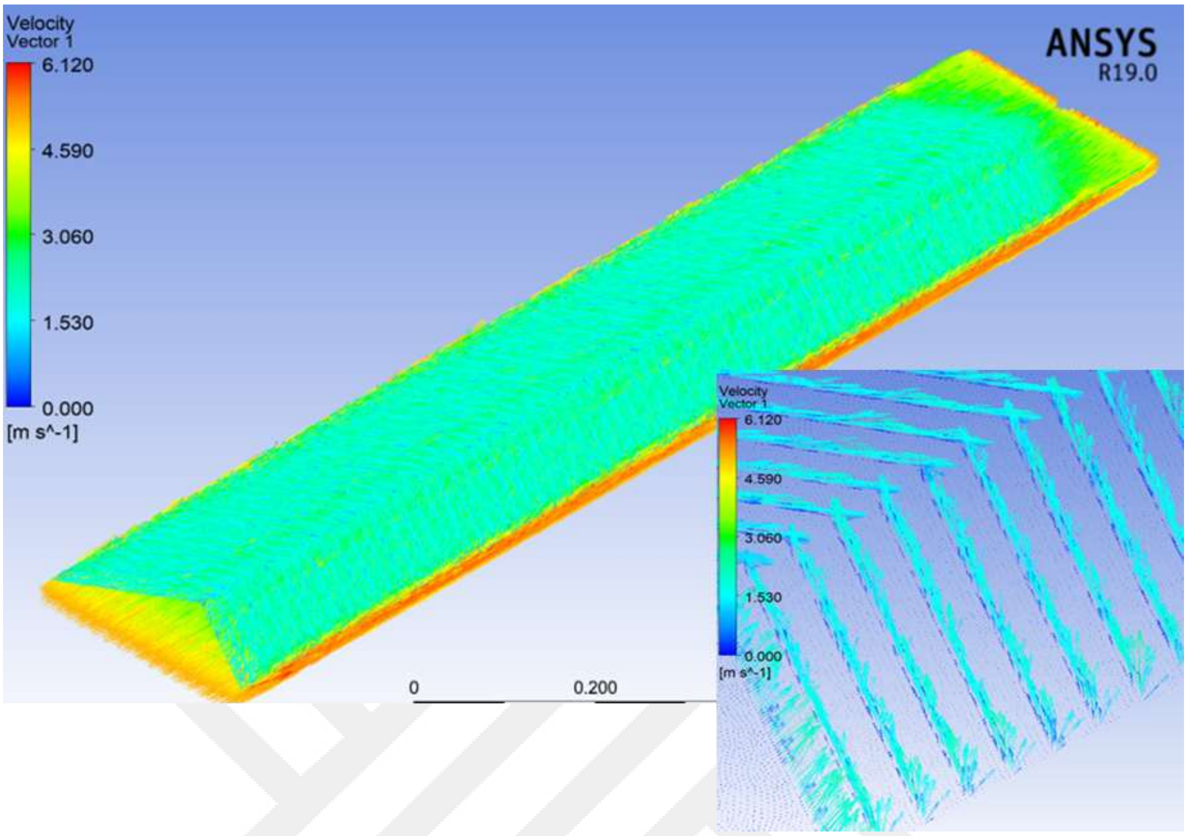

Figure 4.11: Velocity Vector for the Case of Discrete V-ribs with Circular Groove at Re=15,000**.**

4.2.2 Friction Analysis

Figure 4.12 illustrates the variations of the friction factor with Re for roughened plate featuring broken V-shaped ribs, both without grooves and with grooves of semi-circular, triangular, and trapezoidal shapes. The curve for a smooth plate is also included in the figure for comparison purposes.

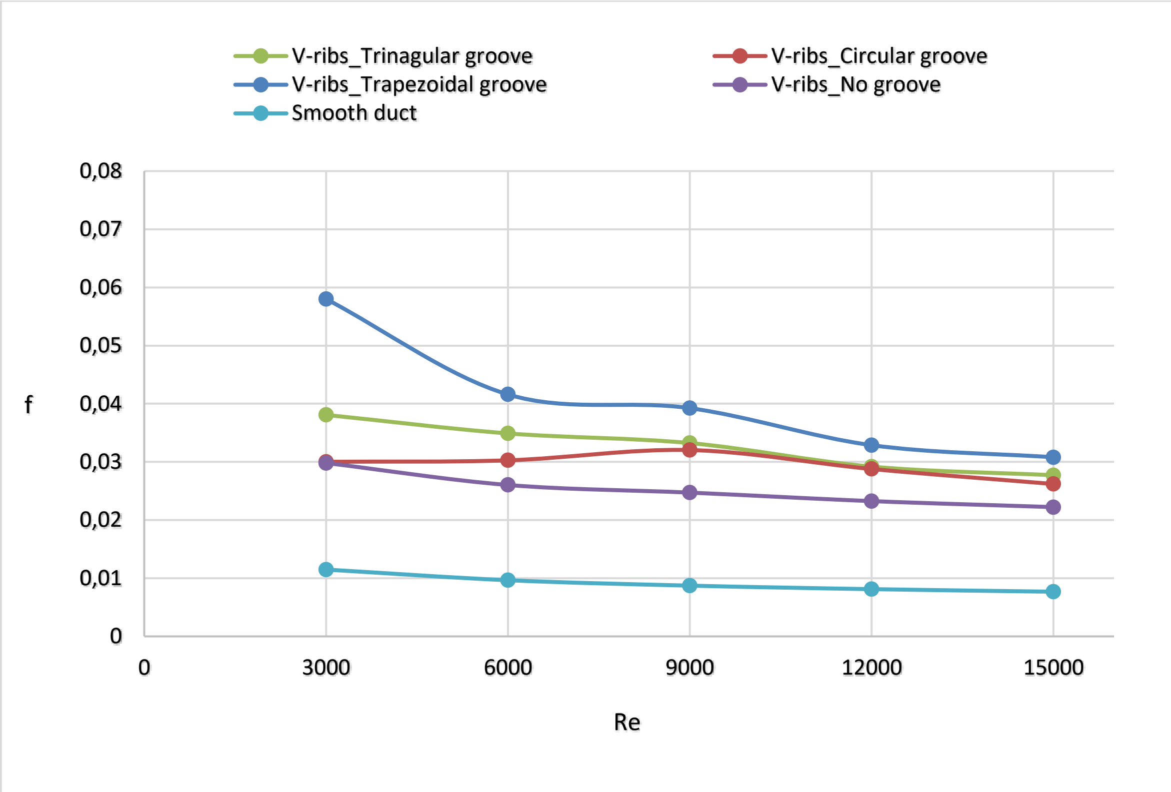

Figure 4.12: Friction Factor Variation of with Re for Broken V-ribs Without Grooves and for the Different Broken V-ribs- Grooves Combinations.

The findings show that for every example this study looked at, friction factors drop as the Reynolds number rises. This expected finding results from the suppression of the viscus sublayer due to increasing Reynolds number values. Combined V-ribs and groove configurations exhibit higher friction factors compared to the case of V-ribs without grooves. This is credited to the enhanced turbulence and flow mixing caused by the presence of grooves. The behavior of friction factor variations with Re as a dependent variable of groove shape differs from that observed for the Nusselt number. While the semi-circular groove provides the maximum heat transfer rates, it results in the lowest friction factor values compared to triangular and trapezoidal grooves shapes. The trapezoidal grooves yield the highest friction factor values. At a Reynolds number of 3,000 the trapezoidal grooves yield a friction factor approximately five times that of a smooth duct and double that of the V-ribs without grooves. The corresponding increases for the triangular grooves are approximately 3.3 and 1.3, respectively, compared to the smooth duct and V-ribs without groove. The friction factor for semi-circular grooves at the same Reynolds number is only slightly higher than that of the V-ribs without groove, but 2.6 times that of the smooth duct. The rounded edges of the semi-circular groove result in smoother turbulent flow, reducing the separation region downstream of the groove and accelerating flow reattachment, which leads to high heat transmission rates and low friction losses.

4.2.3 THPP Analysıs

THPP of the different combinations of V-ribs and grooves considered in the current study is evaluated and presented in figure 4.13. This figure illustrates THPP as a function of Re for V-ribs with semi-circular, triangular, and trapezoidal grooves shapes. THPP variations for the V-ribs case without grooves is also presented in the figure for comparison purposes.

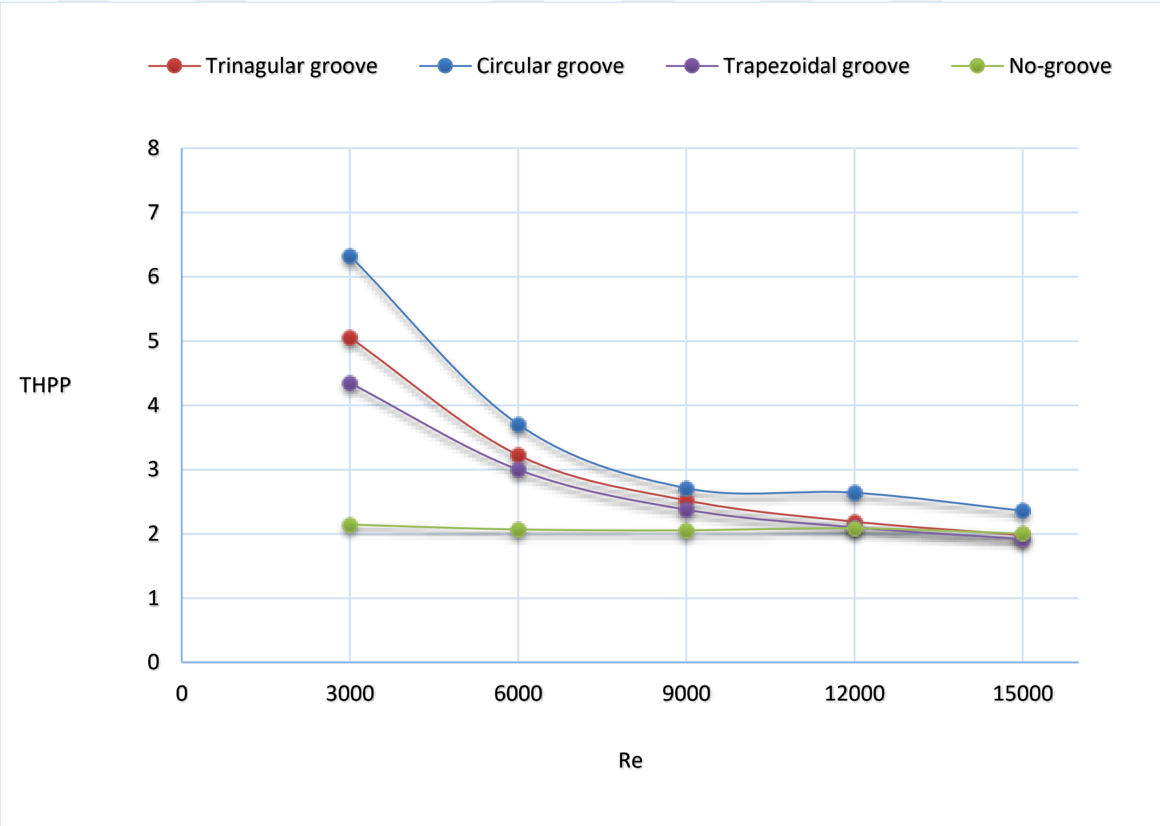

Figure 4.13: THPP Change with Re Number for Broken V-ribs without Grooves and for the Different V-ribs- grooves Combinations

The results reveal that THPP of ducts with V-ribs and groove arrangements, regardless of groove shape, is superior to that with ribs only. Furthermore, it can be observed that THPP for all cases with grooves significantly decreases with increasing Re number. This trend aligns with the numerical data reported by authors in [49], who also used V-ribs with grooves, and with experimental data reported by authors in [74], who employed combined traverse ribs with grooves. The semi-circular grooves yield the best performance, followed by the triangular grooves, and finally the trapezoidal grooves. This is attributed to the high Nusselt numbers and relatively low friction factors observed in the case of semi-circular grooves compared to other cases, as mentioned above. The trapezoidal grooves yield the lowest THPP compared to semi-circular and triangular grooves, due to relatively large friction losses associated with this configuration. The data for the triangular groove lies between the other two ribs-groove configurations considered in this study. THPP values of the optimal roughness arrangement in the present study corresponding to V-ribs with semi-circular grooves, range from 6.3 to 2.4. These values are significantly greater than those in the study in [49], who reported values in the range of 3.2 to 1.8, claiming them as the highest in their study for same range of Re. Consequently, the current roughness arrangement provides optimal performance, and therefore it is recommended for practical applications and future research aimed at further improvements.

5. CONCLUSION AND FUTURE WORK

5.1 CONCLUSION

Attributed to their various applications, like space heating, food drying, desalination, and ventilation and air conditioning, solar air heaters have recently attracted great interest from industrial sectors and researchers. A major challenge associated with traditional smooth SAHs is their low thermal performance, primarily resulted from the presence of a viscus sublayer in contact with the absorber plate. Several techniques have been used to break this sublayer and improve the performance of SAHs. One of the most efficient methods is the employment of artificial roughness with different specifications on the heater plate. Among these, V-shaped roughness designs have been found to provide the best performance compared to other configurations. In present study, a detailed three-dimensional numerical examination of fluid characteristics and heat transmission within a SAH duct is performed using ANSYS fluent software. The purpose is to improve low THPP of the traditional SAH. The study utilizes V-shaped roughness geometries with various configurations, including broken V-ribs pattern, and a combination of V-ribs with grooves patterns, applied to the bottom of the heater plate. Three groove shapes are considered in the study: triangular, semi-circular, and trapezoidal. The dimensions of SAH duct are 1.4 × 0.3× 0.025 m, resulting in AR=12 and a Dh of 0.046 m. The relative roughness parameters are as follows: P/e=1, d/W= 0.65, and relative groove depth (h/e) of 1.

The numerical results obtained in this study include the Nu, friction coefficient, and THPP Additionally, temperature and velocity vectors contours are illustrated for better clarity of results explanation. The investigation is carried out into Re ranged from $3*10^3$ to $15*10^3$. The research's findings allow for the following conclusions to be made:

a. Heat transfer rates are greatly increased by using a variety of V-shaped ribs on the absorber plate of SAH, however this also results in an increase in friction losses. These observations are a result of improved turbulence mixing, vortex production, and separation and reattachment processes.

b. Across all roughness configurations taken into consideration in the study, a rise in the Re results in a noticeable improvement in the friction coefficient and Nu.

c. By adding gaps in the V-ribs pattern, the flow is accelerated and the mixing between the main flow across the ribs downstream of the gaps and the interrupted secondary flow along the ribs is improved. The Nusselt number is increased by up to three times when broken V-ribs are used instead of smooth ducts, which is 30% higher than the value in a continuous V-arrangement.

d. It is discovered that the friction factors in the continuous configuration are three times more than those recorded for a smooth plate, and they are nearly similar to those in broken V-ribs.

e. Depending on the Reynolds number, THPP for the broken V-ribs can range from 2.0 to 2.15, whereas values for the continuous configuration can range from 1.57 to 1.87.

f. Combining grooves with the broken V-ribs roughness results in a significant increment in Nu and friction coefficient. The grooves with a semi-circular cross section provide optimal results, achieving a max. Improvement in the Nu of nearly 1.25, along with a slight raise in friction the factor in comparison to the corresponding V-ribs arrangement without grooves.

g. The triangular and trapezoidal grooves provide approximately a similar increment in the Nu reaching up to 1.05 times that of V-ribs arrangement without grooves. However, there is a large increment in friction factor, particularly with the trapezoidal grooves, reaching up to double the values observed in the corresponding V-ribs arrangement without grooves.

h. The combined V-ribs with grooves arrangements yield thermo-hydraulic factor parameters that are significantly greater than those of other roughness configurations. The maximum values are observed for the V-ribs with semi-circular grooves, ranging from 6.3 to 2.4, depending on the Reynolds number. For triangular and trapezoidal grooves, THPP values range from 5 to 2 and from 4.3 to 1.9, respectively.

5.2 FUTURE WORK

The present study has contributed to enhancing THPP of SAH, but various topics still need to be explored to for further improvements. Based on the current research and its findings, the following recommendations are proposed for future research:

a. Investigate more grooves shapes: Future research should examine additional groove shapes with symmetric and asymmetric cross-sections, to assess their impact on heat and flow measurements. The flow behavior and improvement of heat transmission can be significantly influenced by the grooves' shape.

b. Optimize the position and depth of the grooves: The groove depth and position between the ribs should be optimized to achieve the best performance. These factors can have a significant effect on the boundary sublayer development in the regions before and after the roughness elements, hence affecting heat transfer rate enhancement.

REFERENCES

[1] Y. Goswami, “Energy: the burning issue II,” *Renew. Energy Focus*, vol. 8, no. 4, pp. 68–69, 2007.

[2] S. A. Kalogirou, *Solar energy engineering: processes and systems*. Elsevier, 2023.

[3] W. Weiss and M. Spörk-Dür, “SOLAR HEAT WORLD WIDE: Edition 2023.” AEE—Institute for Sustainable Technologies Gleisdorf, Austria, 2022.

[4] K. G. H. Kong *et al.*, “Shaving electric bills with renewables? A multi-period pinch-based methodology for energy planning,” *Energy*, vol. 239, p. 122320, 2022.

[5] A. Urbina, *Sustainable Solar Electricity*. Springer Nature, 2022.

[6] M. Hadwan and A. Alkholidi, “Solar power energy solutions for Yemeni rural villages and desert communities,” *Renew. Sustain. Energy Rev.*, vol. 57, pp. 838–849, 2016.

[7] “Solar resource maps & GIS data,” *Solargis*, 2024. https://solargis.com/resources/free-maps-and-gis-data.

[8] A. A. El-Sebaii and S. M. Shalaby, “Solar drying of agricultural products: A review,” *Renew. Sustain. Energy Rev.*, vol. 16, no. 1, pp. 37–43, 2012.

[9] A. Vadiee, “The produced hot air can be used in a wide variety of applications, including space heating, food drying, desalination, and ventilation and air conditioning,” in *Solar Energy Advancements in Agriculture and Food Production Systems*, Elsevier, 2022, pp. 237–270.

[10] H.-Y. Chan, S. B. Riffat, and J. Zhu, “Review of passive solar heating and cooling technologies,” *Renew. Sustain. Energy Rev.*, vol. 14, no. 2, pp. 781–789, 2010.

[11] B. kumar Ahirwar, “Review on different techniques used to enhance the thermal performance of solar air heater,” *Int. J. Heat Mass Transf.*, vol. 220, p. 124979, 2024.

[12] V. P. Singh *et al.*, “Recent developments and advancements in solar air heaters: a detailed review,” *Sustainability*, vol. 14, no. 19, p. 12149, 2022.

[13] E. Vengadesan and R. Senthil, “A review on recent developments in thermal performance enhancement methods of flat plate solar air collector,” *Renew. Sustain. Energy Rev.*, vol. 134, p. 110315, 2020.

[14] N. E. Wijeysundera, L. L. Ah, and L. E. Tjioe, “Thermal performance study of two-pass solar air heaters,” *Sol. Energy*, vol. 28, no. 5, pp. 363–370, 1982.

[15] A. A. El-Sebaii, S. Aboul-Enein, M. R. I. Ramadan, S. M. Shalaby, and B. M. Moharram, “Thermal performance investigation of double pass-finned plate solar air heater,” *Appl. Energy*, vol. 88, no. 5, pp. 1727–1739, 2011.

[16] R. Goyal, S. Patel, and A. Sharma, *Renewable Energy: Accelerating the Energy Transition*. Springer, 2023.

[17] S. Panda and R. Kumar, “A review on heat transfer enhancement of solar air heater using various artificial roughed geometries,” *J. Adv. Res. Fluid Mech. Therm. Sci.*, vol. 89, no. 1, pp. 92–133, 2022.

[18] Z. Dong, P. Liu, H. Xiao, Z. Liu, and W. Liu, “A study on heat transfer enhancement for solar air heaters with ripple surface,” *Renew. Energy*, vol. 172, pp. 477–487, 2021.

[19] A. Layek, J. S. Saini, and S. C. Solanki, “Second law optimization of a solar air heater having chamfered rib–groove roughness on absorber plate,” *Renew. Energy*, vol. 32, no. 12, pp. 1967–1980, 2007.

[20] A. K. Patil, J. S. Saini, and K. Kumar, “A comprehensive review on roughness geometries and investigation techniques used in artificially roughened solar air heaters,” *Int. J. Renew. Energy Res.*, vol. 2, no. 1, pp. 1–15, 2012.

[21] K. Thulukkanam, *Heat exchanger design handbook*. CRC press, 2000.

[22] R. P. Saini and S. K. Singal, “A review on roughness geometry used in solar air heaters,” *Sol. energy*, vol. 81, no. 11, pp. 1340–1350, 2007.

[23] V. B. Gawande, A. S. Dhoble, and D. B. Zodpe, “Effect of roughness geometries on heat transfer enhancement in solar thermal systems–A review,” *Renew. Sustain. Energy Rev.*, vol. 32, pp. 347–378, 2014.

[24] I. Singh and S. Singh, "A review of artificial roughness geometries employed in solar air heaters," *Renew. Sustain. Energy Rev.*, vol. 92, pp. 405–425, 2018.

[25] N. Madhukeshwara, "Theoretical and experimental investigations on heat transfer and friction in solar air heater duct with artificial roughness on the absorber surface."

[26] A. Q. Al-Shetwi *et al.*, "Utilization of renewable energy for power sector in Yemen: current status and potential capabilities," *IEEE Access*, vol. 9, pp. 79278–79292, 2021.

[27] S. K. Sharma and V. R. Kalamkar, "Thermo-hydraulic performance analysis of solar air heaters having artificial roughness-A review," *Renewable and Sustainable Energy Reviews*, vol. 41. pp. 413–435, 2015, doi: 10.1016/j.rser.2014.08.051.

[28] S. K. Verma and B. N. Prasad, "Investigation for the optimal thermohydraulic performance of artificially roughened solar air heaters," *Renew. Energy*, vol. 20, no. 1, pp. 19–36, 2000.

[29] M. M. Sahu and J. L. Bhagoria, "Augmentation of heat transfer coefficient by using 90 broken transverse ribs on absorber plate of solar air heater," *Renew. energy*, vol. 30, no. 13, pp. 2057–2073, 2005.

[30] I. Singh, S. Vardhan, S. Singh, and A. Singh, "Experimental and CFD analysis of solar air heater duct roughened with multiple broken transverse ribs: A comparative study," *Sol. Energy*, vol. 188, pp. 519–532, 2019.

[31] D. Gupta, S. C. Solanki, and J. S. Saini, "Heat and fluid flow in rectangular solar air heater ducts having transverse rib roughness on absorber plates," *Sol. energy*, vol. 51, no. 1, pp. 31–37, 1993.

[32] G. Tanda, "Effect of rib spacing on heat transfer and friction in a rectangular channel with 45 angled rib turbulators on one/two walls," *Int. J. Heat Mass Transf.*, vol. 54, no. 5–6, pp. 1081–1090, 2011.

[33] K. R. Aharwal, B. K. Gandhi, and J. S. Saini, "Experimental investigation on heat-transfer enhancement due to a gap in an inclined continuous rib arrangement in a

rectangular duct of solar air heater," *Renew. energy*, vol. 33, no. 4, pp. 585–596, 2008.

[34] T. S. Kumar, V. Mittal, N. S. Thakur, and A. Kumar, "Heat transfer and friction factor correlations for rectangular solar air heater duct having 60 inclined continuous discrete rib arrangement," *Br. J. Appl. Sci. Technol.*, vol. 1, no. 3, pp. 67–93, 2011.

[35] Y. Rathor and K. R. Aharwal, "Heat transfer enhancement due to a staggered element using liquid crystal thermography in an inclined discrete rib roughened solar air heater," *Int. Commun. Heat Mass Transf.*, vol. 118, p. 104839, 2020.

[36] S. C. Lau, R. T. Kukreja, and R. D. McMillin, "Effects of V-shaped rib arrays on turbulent heat transfer and friction of fully developed flow in a square channel," *Int. J. Heat Mass Transf.*, vol. 34, no. 7, pp. 1605–1616, 1991.

[37] J. C. Han, Y. M. Zhang, and C. P. Lee, "Augmented heat transfer in square channels with parallel, crossed, and V-shaped angled ribs," 1991.

[38] R. Kumar *et al.*, "Experimental assessment and modeling of solar air heater with V shape roughness on absorber plate," *Case Studies in Thermal Engineering*, vol. 43. 2023, doi: 10.1016/j.csite.2023.102784.

[39] R. Karwa, "Experimental studies of augmented heat transfer and friction in asymmetrically heated rectangular ducts with ribs on the heated wall in transverse, inclined, V-continuous and V-discrete pattern," *Int. Commun. Heat Mass Transf.*, vol. 30, no. 2, pp. 241–250, 2003.

[40] V. S. Hans, R. P. Saini, and J. S. Saini, "Heat transfer and friction factor correlations for a solar air heater duct roughened artificially with multiple v-ribs," *Sol. energy*, vol. 84, no. 6, pp. 898–911, 2010.

[41] S. Singh, S. Chander, and J. S. Saini, "Heat transfer and friction factor of discrete V-down rib roughened solar air heater ducts," *J. Renew. Sustain. Energy*, vol. 3, no. 1, 2011.

[42] S. Singh, S. Chander, and J. S. Saini, "Heat transfer and friction factor correlations of solar air heater ducts artificially roughened with discrete V-down ribs," *Energy*, vol.

36, no. 8, pp. 5053–5064, 2011.

[43] S. Singh, S. Chander, and J. S. Saini, “Thermo-hydraulic performance due to relative roughness pitch in V-down rib with gap in solar air heater duct—comparison with similar rib roughness geometries,” *Renew. Sustain. Energy Rev.*, vol. 43, pp. 1159–1166, 2015.

[44] A. K. Patil, J. S. Saini, and K. Kumar, “Experimental investigation of enhanced heat transfer and pressure drop in a solar air heater duct with discretized broken V-rib roughness,” *J. Sol. Energy Eng.*, vol. 137, no. 2, p. 21013, 2015.

[45] A. Kumar, R. P. Saini, and J. S. Saini, “Development of correlations for Nusselt number and friction factor for solar air heater with roughened duct having multi v-shaped with gap rib as artificial roughness,” *Renew. Energy*, vol. 58, pp. 151–163, 2013.

[46] R. Maithani and J. S. Saini, “Heat transfer and friction factor correlations for a solar air heater duct roughened artificially with V-ribs with symmetrical gaps,” *Exp. Therm. Fluid Sci.*, vol. 70, pp. 220–227, 2016.

[47] N. S. Deo, S. Chander, and J. S. Saini, “Performance analysis of solar air heater duct roughened with multigap V-down ribs combined with staggered ribs,” *Renew. Energy*, vol. 91, pp. 484–500, 2016.

[48] D. Jin, S. Quan, J. Zuo, and S. Xu, “Numerical investigation of heat transfer enhancement in a solar air heater roughened by multiple V-shaped ribs,” *Renew. Energy*, vol. 134, pp. 78–88, 2019.

[49] A. Kumar and M.-H. Kim, “Heat transfer and fluid flow characteristics in air duct with various V-pattern rib roughness on the heated plate: a comparative study,” *Energy*, vol. 103, pp. 75–85, 2016.

[50] A. Kumar and M.-H. Kim, “Effect of roughness width ratios in discrete multi V-rib with staggered rib roughness on overall thermal performance of solar air channel,” *Sol. Energy*, vol. 119, pp. 399–414, 2015.

[51] D. Jin, J. Zuo, S. Quan, S. Xu, and H. Gao, “Thermohydraulic performance of solar air heater with staggered multiple V-shaped ribs on the absorber plate,” *Energy*, vol. 127, pp. 68–77, 2017.

[52] S. S. Patel and A. Lanjewar, “Experimental and numerical investigation of solar air heater with novel V-rib geometry,” *J. Energy Storage*, vol. 21, pp. 750–764, 2019.

[53] S. S. Patel and A. Lanjewar, “Experimental analysis for augmentation of heat transfer in multiple discrete V-patterns combined with staggered ribs solar air heater,” *Renew. Energy Focus*, vol. 25, pp. 31–39, 2018.

[54] R. K. Ravi and R. P. Saini, “Nusselt number and friction factor correlations for forced convective type counter flow solar air heater having discrete multi V shaped and staggered rib roughness on both sides of the absorber plate,” *Appl. Therm. Eng.*, vol. 129, pp. 735–746, 2018.

[55] P. K. Jain and A. Lanjewar, “Overview of V-RIB geometries in solar air heater and performance evaluation of a new V-RIB geometry,” *Renew. Energy*, vol. 133, pp. 77–90, 2019.

[56] S. S. Patel and A. Lanjewar, “Heat transfer enhancement using additional gap in symmetrical element of V-geometry roughened solar air heater,” *J. Energy Storage*, vol. 38, p. 102545, 2021.

[57] A. Srivastava, G. K. Chhaparwal, and R. K. Sharma, “Numerical and experimental investigation of different rib roughness in a solar air heater,” *Therm. Sci. Eng. Prog.*, vol. 19, p. 100576, 2020.

[58] D. Kumar and A. Layek, “Nusselt number and friction characteristics of solar air heater roughened with novel twisted V-shaped staggered ribs using liquid crystal thermography,” *Renew. Energy*, vol. 201, pp. 651–666, 2022.

[59] U. Allauddin *et al.*, “Numerical investigation of fluid flow and heat characteristics of a roughened solar air heater with novel V-shaped ribs,” *Trans. Can. Soc. Mech. Eng.*, vol. 46, no. 3, pp. 561–572, 2022.

[60] A. Alrashidi, A. A. Altohamy, M. A. Abdelrahman, and I. M. M. Elsemary, “Energy and exergy experimental analysis for innovative finned plate solar air heater,” *Case Stud. Therm. Eng.*, vol. 59, p. 104570, 2024.

[61] P. Raturi, H. Deolal, and S. Kimothi, “Numerical analysis of the return flow solar air heater (RF-SAH) with assimilation of V-type artificial roughness,” *Energy Built Environ.*, vol. 5, no. 2, pp. 185–193, 2024.

[62] S. K. Saini and R. P. Saini, “Development of correlations for Nusselt number and friction factor for solar air heater with roughened duct having arc-shaped wire as artificial roughness,” *Sol. Energy*, vol. 82, no. 12, pp. 1118–1130, 2008.

[63] S. Kumar and R. P. Saini, “CFD based performance analysis of a solar air heater duct provided with artificial roughness,” *Renew. energy*, vol. 34, no. 5, pp. 1285–1291, 2009.

[64] M. K. Sahu and R. K. Prasad, “Thermohydraulic performance analysis of an arc shape wire roughened solar air heater,” *Renew. energy*, vol. 108, pp. 598–614, 2017.

[65] M. K. Sahu and R. K. Prasad, “Exergy based performance evaluation of solar air heater with arc-shaped wire roughened absorber plate,” *Renew. Energy*, vol. 96, pp. 233–243, 2016.

[66] R. S. Gill, V. S. Hans, and S. Singh, “Investigations on thermo-hydraulic performance of broken arc rib in a rectangular duct of solar air heater,” *Int. Commun. Heat Mass Transf.*, vol. 88, pp. 20–27, 2017.

[67] R. S. Gill, V. S. Hans, J. S. Saini, and S. Singh, “Investigation on performance enhancement due to staggered piece in a broken arc rib roughened solar air heater duct,” *Renew. Energy*, vol. 104, pp. 148–162, 2017.

[68] A. P. Singh, “Effect of artificial roughness on heat transfer and friction characteristics having multiple arc shaped roughness element on the absorber plate,” *Sol. energy*, vol. 105, pp. 479–493, 2014.

[69] N. K. Pandey and V. K. Bajpai, “Experimental investigation of heat transfer and

friction characteristics of arc-shaped roughness elements having central gaps on the absorber plate of solar air heater," *J. Sol. Energy Eng.*, vol. 138, no. 4, p. 41005, 2016.

[70] N. K. Pandey and V. K. Bajpai, "Experimental investigation of heat transfer augmentation using multiple arcs with gap on absorber plate of solar air heater," *Sol. Energy*, vol. 134, pp. 314–326, 2016.

[71] R. P. Saini and J. S. Saini, "Heat transfer and friction factor correlations for artificially roughened ducts with expanded metal mesh as roughness element," *Int. J. Heat Mass Transf.*, vol. 40, no. 4, pp. 973–986, 1997.

[72] R. Karwa, S. C. Solanki, and J. S. Saini, "Heat transfer coefficient and friction factor correlations for the transitional flow regime in rib-roughened rectangular ducts," *Int. J. Heat Mass Transf.*, vol. 42, no. 9, pp. 1597–1615, 1999.

[73] J. L. Bhagoria, J. S. Saini, and S. C. Solanki, "Heat transfer coefficient and friction factor correlations for rectangular solar air heater duct having transverse wedge shaped rib roughness on the absorber plate," *Renew. energy*, vol. 25, no. 3, pp. 341–369, 2002.

[74] A. R. Jaurker, J. S. Saini, and B. K. Gandhi, "Heat transfer and friction characteristics of rectangular solar air heater duct using rib-grooved artificial roughness," *Sol. energy*, vol. 80, no. 8, pp. 895–907, 2006.

[75] S. V Karmare and A. N. Tikekar, "Heat transfer and friction factor correlation for artificially roughened duct with metal grit ribs," *Int. J. Heat Mass Transf.*, vol. 50, no. 21–22, pp. 4342–4351, 2007.

[76] R. P. Saini and J. Verma, "Heat transfer and friction factor correlations for a duct having dimple-shape artificial roughness for solar air heaters," *Energy*, vol. 33, no. 8, pp. 1277–1287, 2008.

[77] J. H. Ferziger, M. Perić, and R. L. Street, *Computational methods for fluid dynamics*. springer, 2019.

[78] A. S. Yadav *et al.*, "A Numerical Investigation of an Artificially Roughened Solar Air

Heater," *Energies*, vol. 15, no. 21. 2022, doi: 10.3390/en15218045.

[79] U. Manual, "ANSYS FLUENT 12.0," *Theory Guid.*, vol. 67, 2009.

[80] H. K. Versteeg and W. Malalasekera, *An introduction to computational fluid dynamics: the finite volume method*. Pearson education, 2007.

[81] A. Bejan, *Convection heat transfer*. John wiley & sons, 2013.

[82] S. B. Pope, "Turbulent flows," *Meas. Sci. Technol.*, vol. 12, no. 11, pp. 2020–2021, 2001.

[83] D. C. Wilcox, *Turbulence modeling for CFD*, vol. 2. DCW industries La Canada, CA, 1998.

[84] T. L. Bergman, *Fundamentals of heat and mass transfer*. John Wiley & Sons, 2011.